

## Spatiotemporal characteristics of calcium dynamics in astrocytes

Minchul Kang<sup>1</sup> and Hans G. Othmer<sup>2,a)</sup>

<sup>1</sup>Department of Molecular Physiology and Biophysics, Vanderbilt University School of Medicine, Nashville, Tennessee 37232, USA

<sup>2</sup>School of Mathematics, University of Minnesota, Minneapolis, Minnesota 55455, USA

(Received 21 February 2009; accepted 24 July 2009; published online 18 September 2009)

Although  $\text{Ca}_i^{2+}$  waves in networks of astrocytes *in vivo* are well documented, propagation *in vivo* is much more complex than in culture, and there is no consensus concerning the dominant roles of intercellular and extracellular messengers [inositol 1,4,5-trisphosphate ( $\text{IP}_3$ ) and adenosine-5'-triphosphate (ATP)] that mediate  $\text{Ca}_i^{2+}$  waves. Moreover, to date only simplified models that take very little account of the geometrical structure of the networks have been studied. Our aim in this paper is to develop a mathematical model based on realistic cellular morphology and network connectivity, and a computational framework for simulating the model, in order to address these issues. In the model,  $\text{Ca}_i^{2+}$  wave propagation through a network of astrocytes is driven by  $\text{IP}_3$  diffusion between cells and ATP transport in the extracellular space. Numerical simulations of the model show that different kinetic and geometric assumptions give rise to differences in  $\text{Ca}_i^{2+}$  wave propagation patterns, as characterized by the velocity, propagation distance, time delay in propagation from one cell to another, and the evolution of  $\text{Ca}^{2+}$  response patterns. The temporal  $\text{Ca}_i^{2+}$  response patterns in cells are different from one cell to another, and the  $\text{Ca}_i^{2+}$  response patterns evolve from one type to another as a  $\text{Ca}_i^{2+}$  wave propagates. In addition, the spatial patterns of  $\text{Ca}_i^{2+}$  wave propagation depend on whether  $\text{IP}_3$ , ATP, or both are mediating messengers. Finally, two different geometries that reflect the *in vivo* and *in vitro* configuration of astrocytic networks also yield distinct intracellular and extracellular kinetic patterns. The simulation results as well as the linear stability analysis of the model lead to the conclusion that  $\text{Ca}_i^{2+}$  waves in astrocyte networks are probably mediated by both intercellular  $\text{IP}_3$  transport and nonregenerative (only the glutamate-stimulated cell releases ATP) or partially regenerative extracellular ATP signaling. © 2009 American Institute of Physics. [DOI: 10.1063/1.3206698]

Calcium ( $\text{Ca}^{2+}$ ) is one of the most versatile and widely used second-messenger molecules and plays a pivotal role in neurotransmission, muscle contraction, gene expression, and a variety of other intracellular processes.<sup>13,37</sup>

Because high levels of intracellular calcium are toxic, and because it cannot be degraded as many other signaling molecules are, cells control the intracellular calcium level at around 100 nM (compared to millimolar extracellular levels) by buffering, sequestration in specialized compartments, and by expulsion to the extracellular space.<sup>37,110,115</sup>

In addition to intracellular homeostatic mechanisms to control  $\text{Ca}_i^{2+}$ , sophisticated intracellular signal transduction pathways that involve different proteins modulated by  $\text{Ca}^{2+}$  have evolved for communication between cells.<sup>7,38,39,41,42,60–62,70,100,119</sup>

In the central nervous system, glial cells (collectively, astrocytes, oligodendrocytes, and microglia), which are 10–15 times more numerous than neurons, make up about half of the total brain weight. Astrocytes, which are the dominant glial cell type, had been regarded as maintenance and support cells for neurons until recently, because they lack sodium channels and are electrically nonexcitable.<sup>117</sup> It has been found experimentally that  $\text{Ca}_i^{2+}$  waves propagate through net-

works of astrocytes, and there is a great deal of interest in understanding their role in the brain. In this paper we develop mathematical models that shed light on what factors control the spread of such waves.

### I. INTRODUCTION

#### A. Glutamate induced $\text{Ca}_i^{2+}$ mobilization in astrocytes

A major metabotropic pathway from agonist to calcium changes is via receptor-activated G proteins that initiate production of inositol 1,4,5-trisphosphate ( $\text{IP}_3$ ), which then binds to  $\text{IP}_3$  receptors on calcium channels in the membrane of the endoplasmic reticulum (ER), an intracellular  $\text{Ca}^{2+}$  store. Calcium release from the ER is terminated by  $\text{Ca}^{2+}$  inhibition of channel opening at high concentrations<sup>14</sup> and pumps restore  $\text{Ca}_i^{2+}$  to resting levels. Typically the reuptake makes the  $\text{Ca}^{2+}$  signal a transient “spike” and allows the cell to maintain very low levels of resting  $\text{Ca}_i^{2+}$ .

It was shown previously that the intracellular network that controls  $\text{Ca}_i^{2+}$  dynamics is comprised of four modules [cf. Fig. 1(a)] that can be summarized as follows:<sup>67</sup> (1) the ligand and receptor kinetics at the plasma membrane (the input module), (2) a  $G_q$ -type G-protein-activated module in which activated phospholipase C (PLC) leads to the production of  $\text{IP}_3$  and diacylglycerol (DAG) from phosphatidylinositol-biphosphate ( $\text{PIP}_2$ ) (the amplifying

<sup>a)</sup>Author to whom correspondence should be addressed. Electronic mail: othmer@math.umn.edu. Telephone: +1 (612) 624-8325.

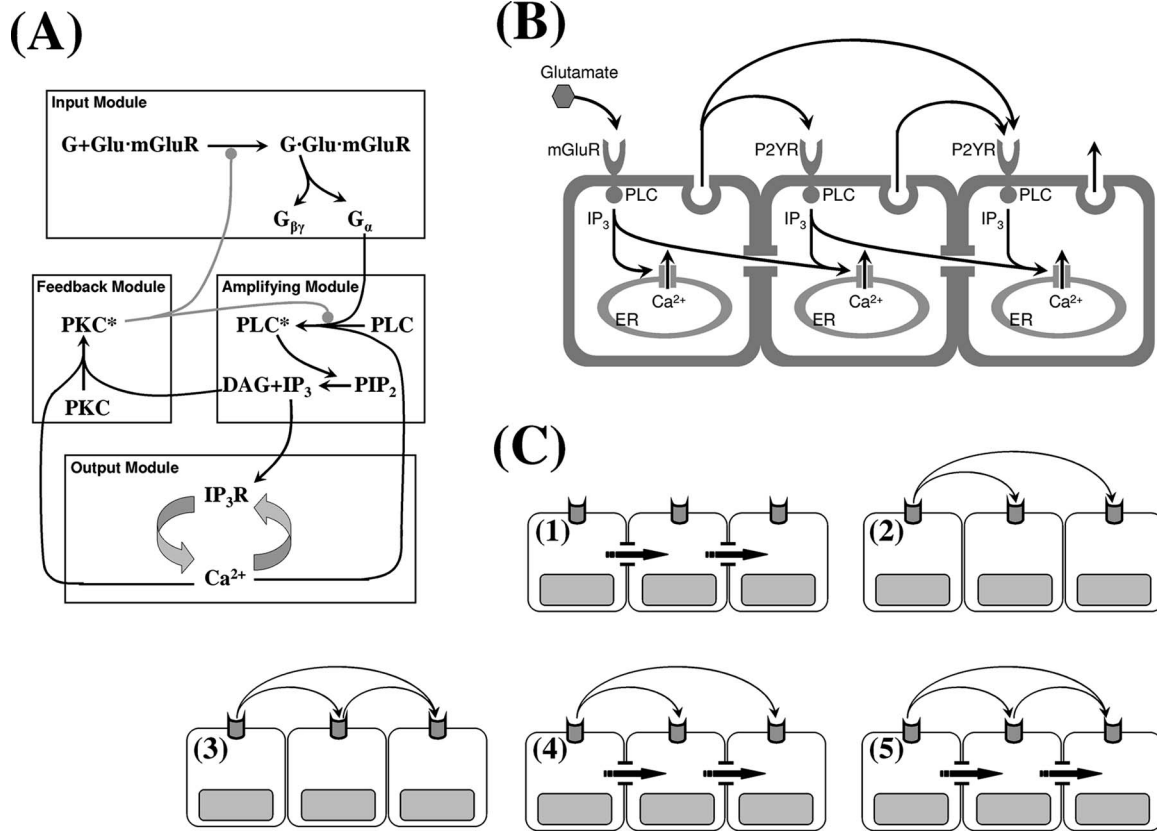


FIG. 1. (a) The modular representation of the glutamate-induced Ca<sup>2+</sup> release pathway. (b) A schematic overview of the possible mechanism of Ca<sup>2+</sup> wave propagation in an astrocyte network. (c) Case studies of Ca<sup>2+</sup> wave propagation under all the possible combination of intracellular and extracellular messengers: (1) direct coupling and no extracellular signal, (2) nonregenerative extracellular signal and no direct coupling, (3) regenerative extracellular signal and no direct coupling, (4) direct coupling and nonregenerative extracellular signal, and (5) regenerative extracellular signal and direct coupling. Note that autocrine ATP signaling is neglected for the glutamate-stimulated cell.

module), (3) an IP<sub>3</sub>/IP<sub>3</sub>-receptor system that controls the Ca<sup>2+</sup> release from the ER by calcium-induced calcium release (CICR) (the output module), and (4) a feedback module involving DAG-Ca<sup>2+</sup> activation of protein kinase C (PKC), which leads to downregulation of receptors and PLC (the feedback module). The input module receives stimulatory ligand and inhibitory PKC signals as inputs and produces G<sub>α</sub> and G<sub>βγ</sub> as outputs, the former of which serves as an input to the amplifying module. The amplifying module produces its outputs, IP<sub>3</sub> and DAG, from the hydrolysis of PIP<sub>2</sub> by G<sub>α</sub>-activated PLC. While soluble IP<sub>3</sub> diffuses into the cytoplasm and functions as an input to the output module, hydrophobic DAG stays at the inner leaflet of the plasma membrane. The output module comprises the Ca<sup>2+</sup> handling mechanisms such as IP<sub>3</sub>-stimulated release from the ER and Sarco/Endoplasmic Reticulum calcium ATPase (SERCA) uptake and outputs Ca<sup>2+</sup>. Finally, the feedback module receives Ca<sup>2+</sup> and DAG as inputs and produces the activated state of PKC, which downregulates the activity of input and amplifying modules. A detailed model for calcium dynamics in isolated cells based on this modular decomposition was derived and analyzed earlier.<sup>67</sup>

### B. Ca<sup>2+</sup> wave propagation in astrocyte networks

It is now believed, after numerous reports of Ca<sup>2+</sup> waves in astrocyte networks following various

stimuli,<sup>89,93,97,84,86,24,45,95</sup> that astrocytes modulate neural network activities via astro-astro and astroneuronal cross-talk, although their physiological roles *in vivo* are still subject to debate.<sup>1,37,45,43,35,83,116,78,99</sup> One example of the cross-talk is reflected in adenosine-5'-triphosphate (ATP)-mediated calcium waves, which demonstrate the coupling between intracellular calcium dynamics and cell-cell communication via the extracellular space.<sup>1,37,56</sup> Such waves, which typically decay in time and in space as they propagate, have a maximal propagation range of 200–350 μm and a maximal velocity of 15–27 μm<sup>2</sup>/s.<sup>15,113,120,82,18</sup>

There is substantial evidence that Ca<sup>2+</sup> waves in astrocytes are mediated by direct coupling between astrocytes via transport through gap junctions<sup>49,105,114,94</sup> and/or by paracrine ATP signaling via the extracellular space.<sup>26,54,18,17,65,103</sup> The mode of communication used depends on the astrocyte subtype,<sup>45</sup> and there is a significant diversity with respect to interactions with surrounding cells.<sup>1</sup> For example, gap junctional coupling appears to be important in astrocytes in the neocortex, while paracrine ATP signaling can induce Ca<sup>2+</sup> waves independent of gap junctional coupling in astrocytes in the hippocampus.<sup>45</sup> However, the findings that Ca<sup>2+</sup> waves can propagate between physically separated astrocytes<sup>54,58,11</sup> and in cultured astrocytes in which gap junctional coupling was pharmacologically impaired<sup>53,63</sup> suggest that extracellular ATP signaling plays a major role in *in vitro*, although it

may not be the only mode. The overview of these possible mechanisms of  $\text{Ca}_i^{2+}$  wave propagation in an astrocyte network is described in Fig. 1(b).

Just as  $\text{Ca}_i^{2+}$  is strictly regulated by cells, the level of ATP is also tightly controlled, but the relative levels are reversed. While cytosolic ATP is  $>5$  mM in most cells,<sup>50,51</sup> extracellular [ATP] is kept around 1 nM (Ref. 64) by various enzymes. Thus large amounts of ATP can be released into the extracellular space under pathological conditions such as tissue injury, cell lysis, and cell ischemia.<sup>3,108</sup> Under physiological conditions, cytosolic ATP can be released via transmembrane transport in response to receptor activation in both vascular smooth muscle cells and endothelial cells.<sup>96,98,68,123</sup> In most neurons, ATP is stored in vesicles with neurotransmitters and coreleased.<sup>16,40</sup> Under experimental conditions various environmental stressors, such as a mechanical stress, have been used as stimuli to release ATP. It has also been reported that ATP may be released via spontaneous changes in cell volume via volume-regulated anion channels (VRACs).<sup>92</sup> Similarly, there are multiple possible ATP release mechanisms in astrocytes. Hemichannel-mediated ATP release,<sup>25,4,103,20,65,2</sup> vesicular release,<sup>22,18,17,122</sup> and P2X7 ATP receptor mediated release<sup>104</sup> have been postulated, but recent evidence suggests that vesicular release is the most probable mechanism.<sup>18,17</sup> At present there is no evidence of transporter-mediated cellular uptake of ATP, even though nucleotides and nucleobases are taken up by several transport systems.<sup>52</sup>

Extracellular ATP can reach biologically active levels from nanomolar to micromolar concentrations near a release site<sup>50,73,82,121</sup> and participates in various signaling processes,<sup>34,32,69</sup> but the half-life of extracellular ATP is very short due to the presence of potent degrading enzymes. It was reported that ATP reaches a local peak as high as 10–75  $\mu\text{M}$  (Refs. 109, 121, and 82) and that the ATP “front” diffuses outward at about 41  $\mu\text{m/s}$ , which exceeds the speed of 28  $\mu\text{m/s}$  for the  $\text{Ca}_i^{2+}$  wave front.<sup>82</sup> The maximal detectable ATP spread ranges from 84 to 120  $\mu\text{m}$  depending on the stimulus source.<sup>82,4,58</sup> The measured diffusion coefficient for the extracellular ATP ranges from 160 to 330  $\mu\text{m}^2/\text{s}$ ,<sup>91,59,81</sup> which is much slower than in the cytosol. Estimated degradation rates for ATP in the extracellular space of astrocytes range from 3.466/s to  $4 \times 10^{-4}/\text{s}$ .<sup>64</sup>

Extracellular ATP can bind to metabotropic ATP receptors (P2YRs) on cells, and at sufficiently high levels it can initiate signaling cascades, including  $\text{Ca}_i^{2+}$  release. The effective dosage of ATP for astrocyte  $\text{Ca}_i^{2+}$  response has been reported to be 0.74–3  $\mu\text{M}$ .<sup>82,64</sup> There are two distinct ATP binding sites on P2YR—low affinity site and high affinity site—the former having a  $K_d=20 \pm 5$   $\mu\text{M}$  with a total concentration of  $B_{\text{max}}=150$  nM/ $10^6$  cells of P2YR, while the latter having a  $K_d=2.5 \pm 0.2$   $\mu\text{M}$  with  $B_{\text{max}}=52$  nM/ $10^6$  cells and a dissociation rate of  $1.2 \times 10^{-3}/\text{s}$ .<sup>76</sup> [Concentrations are based on the volumes of rat and human astrocytes, which have been estimated as  $66 \times 10^3$  and  $18 \times 10^5$   $\mu\text{m}^3$  (Refs. 85 and 21).] In the model we fix the ATP release rate constant so that the peak ATP concentration is  $\sim 30$   $\mu\text{M}$ . Since there are considerable differences in ATP degradation rates reported in the literature, the extracellular

ATP decay rate is treated as a parameter to control the extracellular ATP level. For simplicity, we will not distinguish the two different ATP binding sites on P2YR and set  $B_{\text{max}}=0.1$   $\mu\text{M}$  and  $K_d=10$   $\mu\text{M}$ .

### C. The rationale for the model structure

$\text{Ca}_i^{2+}$  increases are often found to be spatially synchronized in cultured astrocytes, which usually form an adherent cell monolayer that is well approximated as a rectangular tessellation of a two-dimensional (2D) domain.<sup>37,45,11</sup> This has led to suggestions that long-range propagation of  $\text{Ca}_i^{2+}$  in cultured astrocytes is doubtful under physiological conditions.<sup>45,1</sup> However, *in vivo* astrocytes are interconnected by well-developed fine processes that constrain the waves to propagate along certain routes and provide weaker gap-junctional connectivity between cells. Even for the same cell type, differences exist between cultured astrocytes and astrocytes *in vivo*, and as a result, there are conflicting opinions concerning the roles played by intercellular and extracellular messengers in astrocytic  $\text{Ca}_i^{2+}$  waves. As we show later, using a realistic morphology has important implications for complex network dynamics, although other factors also have significant effects. Our results suggest that morphological differences in cultured and intact astrocytes can cause different  $\text{Ca}_i^{2+}$ ,  $\text{IP}_3$ , and ATP wave propagation patterns in terms of propagation velocity, propagation distance, amplitude, and delays between cells.

Many theoretical studies have been done to understand the phenotypical properties of  $\text{Ca}_i^{2+}$  waves reported for different cell types in various contexts.<sup>60,10</sup> For example, it is known how to predict the range of propagation in a highly simplified model of gap-junction-coupled cells.<sup>5</sup> However, to our knowledge no studies have considered realistic morphological differences between cells in different experimental studies. We considered a realistic yet simple mathematical model of  $\text{Ca}_i^{2+}$  elevation and wave propagation in two different geometries mimicking astrocytic networks *in vivo* and *in vitro* and tested it under various scenarios of  $\text{Ca}_i^{2+}$  wave propagation [Fig. 1(c)] based on a number of simplifying assumptions. First, we assumed that sustained glutamate stimulus is locally restricted in one cell, yet the glutamate concentration is high enough so that ATP released from neighboring astrocytes does not influence the  $\text{Ca}_i^{2+}$  response kinetics in the glutamate-stimulated cell. Second, all the astrocytes share identical physiological properties, which means that the same system of partial differential equations (PDEs) is valid for all the cells. Third, the distribution of ER is homogeneous throughout the cell body and processes of an astrocyte, i.e., the shape of the ER network matches the shape of an astrocyte. Fourth, P2YRs are also uniformly distributed over the cell body and processes of an astrocyte, and gap junctions may exist between adjacent astrocytes. Finally, we assume that the only difference between astrocytes *in vivo* and *in vitro* is in their morphology.

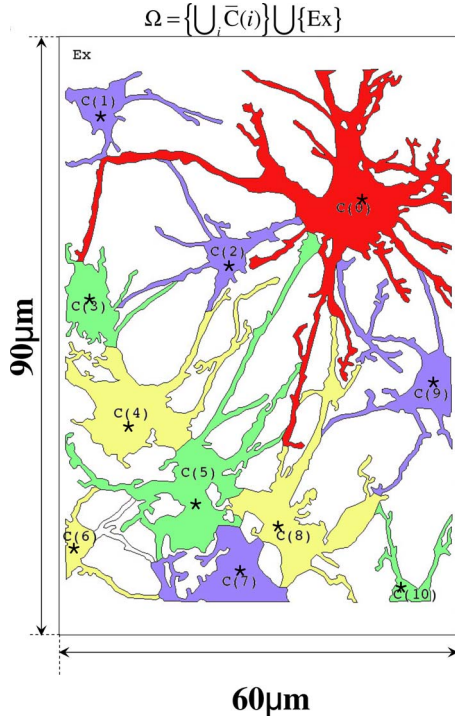


FIG. 2. (Color online) The astrocytic network geometry used in the *in vivo* model. Here and in the simplified model,  $C(0)$  is the cell stimulated by glutamate. The extracellular space is defined as  $\Omega = \{\cup_i \bar{C}(i)\} \cup \{Ex\}$ , where  $\bar{C}(i)$  is the extracellular domain above  $C(i)$  and  $Ex$  is the cell free space.

## II. THE MATHEMATICAL MODEL FOR $Ca_i^{2+}$ WAVES

### A. An overview of the spatial model

In the previous study,<sup>67</sup> a model of ligand-induced intracellular  $Ca_i^{2+}$  oscillations was developed and analyzed to understand the bifurcation structure of the different types of  $Ca_i^{2+}$  oscillations, particularly sinusoidal  $Ca_i^{2+}$  oscillations and baseline spiking, in terms of the role of PKC and PLC in determining the intracellular level of  $IP_3$ . Our objective here is to extend this to allow different modes of cell-cell communication, either directly via gap junctions or indirectly via the extracellular space. The goal is to develop a PDE model in order to understand  $Ca_i^{2+}$  wave propagation through an astrocytic network and ATP wave propagation in the extracellular space. As previously mentioned, substantial differences in  $Ca_i^{2+}$  waves were reported among different subtypes of astrocytes that result from the diversity of interactions with surrounding cells.<sup>45</sup> The differences are even larger between astrocytes *in vitro* (cultured) and *in vivo*.<sup>45</sup>

To determine how the different configurations of astrocyte network geometries influence  $Ca_i^{2+}$  wave propagation, the PDE model must be solved numerically in both realistic (*in vivo*) and simplified (*in vitro*) geometries for astrocyte networks, assuming only morphological differences between cultures and intact astrocytes (Fig. 2). In both cases, simulations under all possible combinations of direct coupling using an intracellular messenger ( $IP_3$ ) and indirect communication using an extracellular messenger (ATP) were done to study the properties of  $Ca_i^{2+}$  waves. The cases considered are (1) direct coupling and no extracellular signal, (2) nonregenerative extracellular signal and no direct coupling, (3) regen-

erative extracellular signal and no direct coupling, (4) direct coupling and nonregenerative extracellular signal, and (5) regenerative extracellular signal and direct coupling [Fig. 1(c)].

### B. Simplification of the intracellular temporal model

It can be shown that the full temporal model studied earlier<sup>67</sup> can be reduced to interactions between the key component in each of the modules, namely,  $IP_3$ ,  $IP_3R$ ,  $Ca^{2+}$ , and PKC. Formally, this can be done by introducing a time scale  $\bar{t} = k_{-RCC}t$ , converting the ordinary differential equation (ODE) system into nondimensional form to identify fast and slow steps as measured by the sizes of nondimensional groups and applying the pseudosteady state hypothesis to reduce some ODEs to algebraic equations.<sup>47,66</sup> By simplifying the resulting algebraic-differential equations we obtain a system that captures the slow dynamics to leading order in the small parameter. This leads to the following four-dimensional system:

$$\frac{dP}{dt} = \frac{k_1 C}{(1 + k_2 K)} - k_3 P,$$

$$\frac{dK}{dt} = k_4 C(K_T - K) - k_5 K,$$

$$\frac{dR}{dt} = \frac{k_6 P C^2 (R_T - R)}{1 + k_7 P (1 + k_8 C)} - k_9 R,$$

$$\frac{dC}{dt} = k_{10} \left( 1 + \frac{k_{11} P C (R_T - R)}{1 + k_7 P (1 + k_8 C)} \right) (k_c - C) - \frac{k_{12} C^2}{C^2 + k_p^2},$$

where  $P$ ,  $K$ ,  $R$ , and  $C$  represent the concentrations of  $IP_3$ ,  $Ca^{2+} \cdot PKC$  complex,  $Ca^{2+} \cdot Ca^{2+} \cdot IP_3 \cdot IP_3R$ , and  $Ca_i^{2+}$ . The parameters that appear in Eq. (1) are given in Table I. Notice that  $C$  couples the first two equations to the last two, whereas  $P$  couples the last two to the first two. The reader can interpret the equations in terms of the interactions between the modules. For example,  $K$ , which arises from the feedback, affects the output via the first term in the first equation. The inhibitory feedback pathway of PKC  $Ca_i^{2+}$  dynamics is well documented in various studies.<sup>8,30,31,29,112,6,28,46,23,80</sup> Further discussion of the physical interpretation of Eq. (1) can be found in Appendix A and Ref. 66.

### C. Geometry of the astrocyte networks

We later derive equations for waves in cultured astrocytes and for *in vivo* networks and here describe the geometry we use. Cultured astrocytes are often confluent, and to understand waves in this context we consider a finite line of cells wherein each is coupled to its nearest neighbors via gap junctions, as shown in Fig. 1(b). This line of cells is covered by a thin extracellular space that extends above and to the end of the line, in which ATP can diffuse, and we homogenize this system in the vertical direction so as to reduce it to 2D system of coupled squares of  $15 \times 15 \mu m^2$  with fluid layer above it. We solve the equations both within the squares and in the exterior fluid layer using equations and

TABLE I. Parameters and their meaning. In the simplified geometry (*in vitro* model),  $k_{\text{perm } p=1}$  were used (\*). For  $\text{IP}_3$  mediated  $\text{Ca}_i^{2+}$  wave (without ATP binding kinetics),  $k_{\text{in}}=0$  was chosen ( $\dagger$ ), while  $k_{\text{perm } p=0}$  was used to study ATP mediated  $\text{Ca}_i^{2+}$  wave without  $\text{IP}_3$  diffusion ( $\ddagger$ ).

Parameter	Unit	Meaning	Value
$D_A$	$\mu\text{m}^2 \text{sec}^{-1}$	Diffusion coefficient of ATP in extracellular space	330
$D_P$	$\mu\text{m}^2 \text{sec}^{-1}$	Diffusion coefficient of $\text{IP}_3$	300
$D_K$	$\mu\text{m}^2 \text{sec}^{-1}$	Diffusion coefficient of $\text{Ca}^{2+}\cdot\text{PKC}$	30
$D_C$	$\mu\text{m}^2 \text{sec}^{-1}$	Effective diffusion coefficient of $\text{Ca}_i^{2+}$	30
$k_1$	$\text{sec}^{-1}$	$\text{Ca}^{2+}$ dependence of $\text{IP}_3$ production	4.7994
$k_2$	$\mu\text{M}^{-1}$	PKC dependence of $\text{IP}_3$ production	0.0943
$k_3$	$\text{sec}^{-1}$	$\text{IP}_3$ degradation rate	2.5000
$k_4$	$\mu\text{M}^{-1} \text{sec}^{-1}$	Rate constant for PKC and $\text{Ca}^{2+}$ binding	0.6000
$k_5$	$\text{sec}^{-1}$	$K(\overline{\text{Ca}^{2+}}\cdot\text{PKC})$ degradation rate	0.5000
$k_6$	$\mu\text{M}^{-2} \text{sec}^{-1}$	Binding rate constant for $\text{IP}_3, 2\text{Ca}^{2+}$	139.09
$k_7$	$\mu\text{M}^{-1}$	Affinity constants for $\text{IP}_3, \text{IP}_3\text{R}$	8.5000
$k_8$	$\mu\text{M}^{-1}$	Affinity constants for $\text{Ca}^{2+}, \text{IP}_3\cdot\text{IP}_3\text{R}$	9.0909
$k_9$	$\text{sec}^{-1}$	$R(\text{IP}_3\cdot\text{IP}_3\text{R}\cdot\text{Ca}^{2+}\cdot\text{Ca}^{2+})$ degradation rate	0.2100
$k_{10}$	$\text{sec}^{-1}$	Basal $\text{Ca}^{2+}$ release rate from ER	0.0185
$\tilde{k}_{11}$	$\mu\text{M}^{-2}$	Affinity constant for $C, P,$ and free $\text{IP}_3\text{R}$	.
$\bar{k}_{11}$	$\mu\text{M}^{-1} \text{sec}^{-1}$	$\text{Ca}^{2+}$ release rate from $\text{IP}_3\text{R } \text{Ca}^{2+}$ channels	.
$k_{11}$	$\mu\text{M}^{-3}$	$\bar{k}_{11}\tilde{k}_{11}/k_{10}$	15841
$k_{12}$	$\mu\text{M} \text{sec}^{-1}$	The maximal $\text{Ca}^{2+}$ pumping rate	7.5000
$k_c$	$\mu\text{M}$	Volume averaged $\text{Ca}^{2+}$ concentration	7.0000
$k_{p2}$	$\mu\text{M}$	$\text{Ca}^{2+}$ sensitivity of the SERCA pump	0.1300
$K_T$	$\mu\text{M}$	Total $K$ concentration	1.0000
$R_T$	$\mu\text{M}$	Total $R$ concentration	0.8000
$A_T$	$\mu\text{M}$	ATP concentration in the cytosol	5000
$k_{\text{in}}$	$\text{sec}^{-1}$	Rate of ATP induced $\text{IP}_3$ production	$30/0^\dagger$
$k_{\text{-ATP}}$	$\text{sec}^{-1}$	ATP decay rate in extracellular space	1
$B_{\text{max}}$	$\mu\text{M}$	The total concentration of P2YR	0.1
$K_d$	$\mu\text{M}$	Dissociation constant of ATP and P2YR	10
$k_{\text{ATP}}$	$\text{sec}^{-1}$	Maximal ATP release rate	0.184
$\gamma$	$\mu\text{m}^{-1}$	Extracellular volume dependent parameter	1.087
$\rho$	$\mu\text{M}$	$\text{IP}_3$ dependency parameter in ATP release	10
$k_{\text{perm } p}$	$\mu\text{m/s}$	Gap junctional permeability for $\text{IP}_3$	$2/1^*/0^\ddagger$
$L$	$\mu\text{m}$	The height of extracellular space	0.9

boundary conditions given later. Similar simplified model geometry was also studied extensively in Refs. 11, 101, 102, and 12.

The geometry of a realistic *in vivo* astrocyte network is very complicated, as shown in Fig. 2, and some simplifications are necessary. From the morphological point of view, astrocytes *in vivo* have well developed processes in both number and size covering most of the dendrites, axons, and synapses, as well as the larger soma.<sup>1,21,85</sup> To capture these characteristics, a realistic astrocyte network in  $60 \times 90 \mu\text{m}^2$  rectangular domain was considered which was modified from original confocal immunofluorescence images of the vitreal surface of the rat retina.<sup>81</sup> The locations at which  $C_i, P_i,$  and  $A$  in  $C(i)$  were measured were marked as  $\star$  [Fig. 2(b)], where  $A$  represents extracellular ATP concentration. The distance between measuring point from  $C(0)$  in descending order are  $C(2), C(9), C(1), C(3), C(4), C(8), C(5), C(10), C(7),$  and  $C(6)$  with distances 20.3, 29.8, 40.4, 42.4, 46.4, 49.3, 50.3, 58.2, 59.3, and 64.76 ( $\mu\text{m}$ ). This system is also treated as having been homogenized the vertical direction, and equations given later are solved in the domain defined by the cells and that defined by the extracellular

space. Here there is an additional difficulty, in that to be entirely faithful to the *in vivo* geometry we should treat the system as a two phase system (cell and fluid) as above, but here the fraction of the phases varies from point to point. This extension significantly complicates the problem computationally, and this will be pursued elsewhere.

Several lines of evidence indicate that gap junctional hemichannels play an important role by providing a direct path to second messengers such as  $\text{IP}_3$ .<sup>15,49,72,105,114</sup> A portion of mobilized  $\text{Ca}_i^{2+}$  also diffuses through the gap junctional hemichannels. However, due to various of  $\text{Ca}^{2+}$  buffer proteins in the cytosol, the amount is negligible and we ignore diffusion of  $\text{Ca}_i^{2+}$  between cells.<sup>110,9</sup> We assume that astrocytic gap junctions are located at the end of astrocytic processes as well as on the part of the boundary where astrocyte bodies.<sup>79</sup> Because it was hard to distinguish different cells from the image, the cell boundaries other than processes in the model were simply assigned. It was also assumed that the ATP receptors are present over the entire cell surface, although some studies indicate that a localization of ATP receptors either in an astrocyte cell body or processes could be specific to the astrocyte subtype.<sup>48,90</sup>

#### D. The governing equations for the spatial model

Let  $C(0)$  be a cell stimulated by glutamate (parametrized by  $k_1$ ) and  $C(i)$ ,  $i \neq 0$  be the surrounding cells (Fig. 2), and let  $X_i$  denote a quantity  $X$  in the  $i^{\text{th}}$  cell. In the subdomain  $C(0)$  (Fig. 2), for  $t > 0$ ,

$$\begin{aligned} \frac{\partial P_0}{\partial t} &= D_P \Delta P_0 + \frac{k_1 C_0}{1 + k_2 K_0} - k_3 P_0 \\ \frac{\partial K_0}{\partial t} &= D_K \Delta K_0 + k_4 C_0 (K_T - K_0) - k_5 K_0, \\ \frac{\partial R_0}{\partial t} &= \frac{k_6 P_0 C_0^2 (R_T - R_0)}{1 + k_7 P_0 (1 + k_8 C_0)} - k_9 R_0, \\ \frac{\partial C_0}{\partial t} &= D_C \Delta C_0 + k_{10} \left( 1 + \frac{k_{11} C_0 P_0 (R_T - R_0)}{1 + k_7 P_0 (1 + k_8 C_0)} \right) (k_c - C_0) \\ &\quad - \frac{k_{12} C_0^2}{C_0^2 + k_{p2}^2}, \end{aligned} \quad (2)$$

where  $R_0$  is assumed to be immobile ( $D_R=0$ ). The initial conditions on  $C(0) \times \{t=0\}$  are given by

$$\begin{aligned} P_0(x, 0) &= 0 \quad K_0(x, 0) = 0 \\ R_0(x, 0) &= 0 \quad C_0(x, 0) = 0.02. \end{aligned} \quad (3)$$

Wherever cell  $C(0)$  meets other cells we impose the boundary conditions

$$\begin{aligned} -D_P \frac{\partial P_0}{\partial n} &= k_{\text{perm}} P_0 (P_0 - P_i), \\ \frac{\partial X}{\partial n} &= 0 \quad \text{for } X = K_0, R_0, C_0, \end{aligned} \quad (4)$$

while all other boundaries are impermeable to all species. When we consider extracellular messenger-mediated  $\text{Ca}_i^{2+}$  waves without  $\text{IP}_3$  diffusion between cells, we simply set  $k_{\text{perm}} P_0 = 0$ .

Since ATP affects  $\text{Ca}^{2+}$  wave propagation via binding to P2YR, the equation for  $\text{IP}_3$  involves an input that depends on ATP binding kinetics ( $B_{\text{max}}=0.1 \mu\text{M}$ ,  $K_d=10 \mu\text{M}$ ) as well as on  $\text{Ca}_i^{2+}$  ( $C_i$ ) and PKC ( $K_i$ ). A similar term is absent from the glutamate-stimulated cell because we neglect the ATP stimulation relative to that by glutamate. Therefore,

$$\begin{aligned} \frac{\partial P_i}{\partial t} &= D_P \Delta P_i + k_{\text{in}} \frac{B_{\text{max}} A}{K_d + A} \frac{C_i}{1 + k_2 K_i} - k_3 P_i, \\ \frac{\partial K_i}{\partial t} &= D_K \Delta K_i + k_4 C_i (K_T - K_i) - k_5 K_i, \\ \frac{\partial R_i}{\partial t} &= \frac{k_6 P_i C_i^2 (R_T - R_i)}{1 + k_7 P_i (1 + k_8 C_i)} - k_9 R_i, \end{aligned} \quad (5)$$

$$\begin{aligned} \frac{\partial C_i}{\partial t} &= D_C \Delta C_i + k_{10} \left( 1 + \frac{k_{11} C_i P_i (R_T - R_i)}{1 + k_7 P_i (1 + k_8 C_i)} \right) (k_c - C_i) \\ &\quad - \frac{k_{12} C_i^2}{C_i^2 + k_{p2}^2}, \end{aligned}$$

with initial conditions and boundary conditions. Notice that the glutamate-dependent source term in  $P_0(k_1)$  is replaced by the ATP-dependent term  $k_{\text{in}} B_{\text{max}} A / (K_d + A)$  in  $P_i$  for  $i \neq 0$ . When  $\text{Ca}_i^{2+}$  waves are mediated only by the intracellular messenger ( $\text{IP}_3$ ), we set  $k_{\text{in}}=0$  in  $C(i)$  for  $i \neq 0$ .

On the other hand, ATP kinetics are defined domainwise in the extracellular space,  $\bar{\Omega} = \{\cup_i \bar{C}(i)\} \cup \{\text{Ex}\}$  with the boundary  $\partial\bar{\Omega}$  (Fig. 2), where  $\bar{C}(i)$  is a domain right above  $C(i)$  in extracellular space and Ex is cell-free extracellular space. Notice that  $\partial\bar{\Omega}$  consists of four sides of the rectangular  $\bar{\Omega}$  in the realistic geometry [Fig. 2(b)], while  $\partial\bar{\Omega}$  is found at both sides of the simplified geometry [Fig. 2(a)]. In  $\bar{C}(i)$ , with an extracellular volume dependent parameter  $\gamma$ , the equation of ATP kinetics (see Appendix B for more details) is

$$\frac{\partial A}{\partial t} = D_A \frac{\partial^2 A}{\partial x^2} - k_{\text{-ATP}} A + \gamma k_{\text{ATP}} \phi(P_i) (A_T - A), \quad (6)$$

where  $A_T$  is the intracellular concentration of ATP with the initial condition

$$A(x, 0) = 0.$$

The function  $\phi$  describes ATP release kinetics either by hemichannels or by vesicular release. Because  $\phi$  is unknown, we choose  $\phi(P_i) = P_i / (\rho + P_i)$  for some constant  $\rho$  (Table I). It should be noted that a recent study<sup>118</sup> suggested that  $\phi$  is a bell-shaped function of  $[\text{Ca}_i^{2+}]$ , but we assumed that ATP release is triggered by  $\text{IP}_3$ .<sup>20,22</sup>

On the other hand, for nonregenerative ATP release [Fig. 1(C2), (C4)], there is no source term in any but the glutamate-stimulated cell, and thus  $k_{\text{ATP}}=0$  in Eq. (6) for  $C(i)$ ,  $i \neq 0$ . This applies in the cell-free region as well. In all cases, we use the boundary condition on  $\partial\bar{\Omega}$  as  $D(\partial A / \partial n) = -A$  to reflect leakage of ATP to the surroundings [Fig. 2(c)].

For the numerical computations, Eqs. (2)–(6) in the domains in Fig. 2 were solved by the finite element method implemented by FEMLAB<sup>®</sup> with a choice of linear Lagrangian interpolation for the shape functions. The system of PDEs described on geometries defined in Fig. 2 was incorporated into FEMLAB and UMFPAK (Ref. 33) was chosen to solve the resulting nonsymmetric, sparse linear systems.

### III. RESULTS AND DISCUSSION

#### A. $\text{Ca}^{2+}$ wave propagation and evolution of $\text{Ca}_i^{2+}$ response patterns in a network of cells

In a previous study it was demonstrated that the different  $\text{Ca}_i^{2+}$  response types are determined by  $[\text{IP}_3]$ , which, in turn, is controlled by the activities of PLC and PKC.<sup>67</sup> The effect of  $[\text{IP}_3]$  on the complexity of calcium oscillations in a single cell was also addressed by Pittà *et al.*<sup>88</sup> in a simpler framework. Since  $\text{IP}_3$  levels are different from one cell to another in an astrocytic network, we may expect different types of

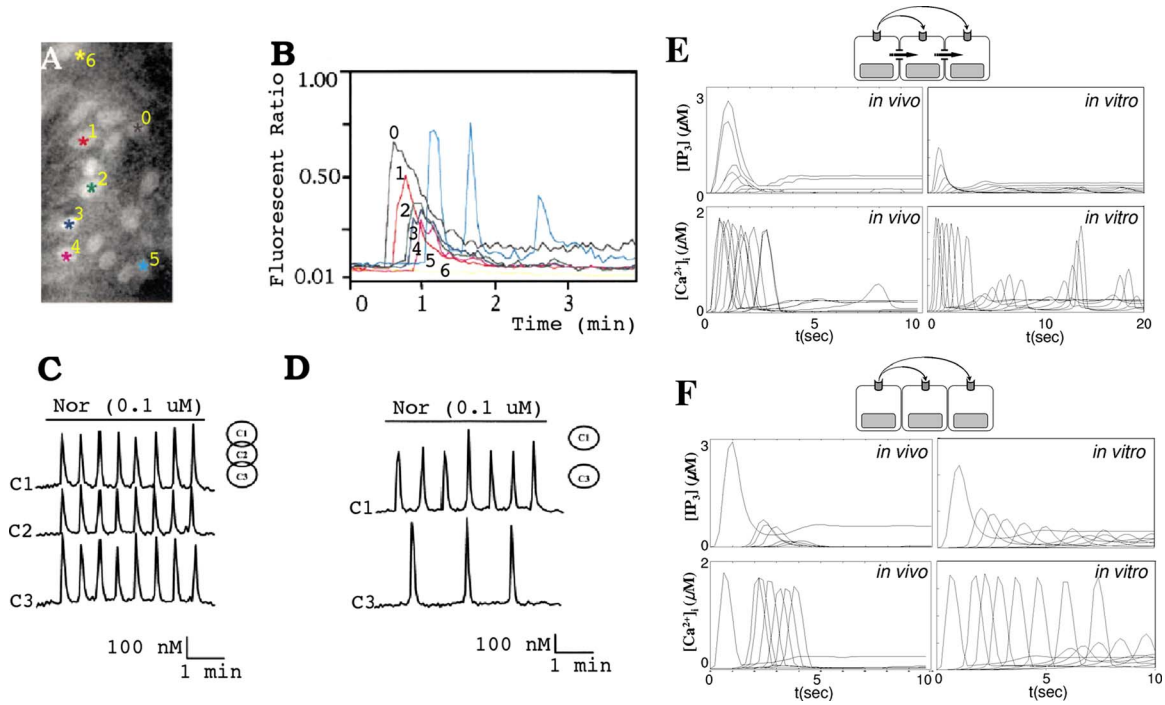


FIG. 3. (Color online) Evolution of the  $\text{Ca}_i^{2+}$  response types in cells. [(a) and (b)] Distribution and pattern of  $\text{Ca}_i^{2+}$  responses to focal application of receptor agonist in rat astrocytes in a  $200 \times 100 \mu\text{m}^2$  rectangle (Ref. 113). [(c) and (d)] Noradrenaline-induced  $[\text{Ca}_i^{2+}]$  oscillation in rat hepatocytes when three cells are connected and when the intermediate cell was excised (Ref. 111). [(e) and (f)] Simulation results from simplified geometry (*in vitro*) and realistic geometry (*in vivo*) corresponding to (a), (b) and (c), (d). The traces from left to right in (e) (*in vivo*)  $[\text{Ca}_i^{2+}]$  correspond to  $C(i)$ ,  $i=0, 1, 3, 2, 9, 4, 8, 5, 7, 6$ , and 10 in descending order. The traces from left to right in (f) (*in vivo*)  $[\text{Ca}_i^{2+}]$  correspond to  $C(i)$ ,  $i=0, 2, 9, 1, 5, 8, 4$  with subthreshold  $\text{Ca}_i^{2+}$  responses in  $C(3)$  and  $C(10)$ . The traces from top to bottom in (e)  $[\text{IP}_3]$  correspond to  $C(i)$ ,  $i=1, 0, 2, 3, 9, 4, 8, 5, 7, 6$ , and 10 in descending order. Also, in (f),  $[\text{IP}_3]$ , the traces from top to bottom correspond to in  $C(i)$ ,  $i=0, 2, 9, 1, 5, 8, 4$ , and 7 in descending order and  $[\text{IP}_3] \approx 0$  in  $C(3)$  and  $C(10)$ . In (e) (*in vitro*) and (f) (*in vitro*), the traces from top to bottom are  $C(i)$ ,  $i=0, \pm 1, \pm 2, \dots, \pm 7$ .

$\text{Ca}_i^{2+}$  response in different cells. Indeed Venance *et al.*<sup>113</sup> reported an evolution of  $[\text{Ca}_i^{2+}]$  response patterns in rat astrocytes [Figs. 3(a) and 3(b)]. In Figs. 3(a) and 3(b), cells 1–4 show a gradual change from a “transient with plateau-type” response pattern (cell 0) to a “transient without plateau-type” response pattern. Interestingly, the beginnings of a baseline spiking-type response pattern were observed in the fifth cell, whereas the sixth showed no response.

Another interesting observation was made by Tordjmann *et al.*,<sup>111</sup> who found that noradrenaline-induced  $[\text{Ca}_i^{2+}]$  oscillation patterns in three interconnected rat hepatocytes were similar, whereas different  $\text{Ca}_i^{2+}$  patterns were observed in the first and third cells when those cells were physically separated by excising the intermediate second cell, thereby presumably removing direct coupling through gap junctions. Also, longer delays in the initial  $\text{Ca}_i^{2+}$  transients were observed in the latter case [Figs. 3(c) and 3(d)]. (Here one must be careful when  $\text{Ca}_i^{2+}$  dynamics in hepatocytes and astrocytes are compared because  $\text{Ca}_i^{2+}$  waves in hepatocytes are predominantly carried by  $\text{IP}_3$  through intercellular gap junctions<sup>111</sup> while both intracellular  $\text{IP}_3$  and extracellular messengers are believed equally importantly in  $\text{Ca}_i^{2+}$  waves in astrocytes.<sup>53,25,27,26,54,44</sup>)

To determine whether the model can reproduce the results in Figs. 3(a)–3(d), Eqs. (2)–(6) were solved numerically on the geometries (Fig. 2) under the assumption of either only an intracellular messenger and nonregenerative extracellular messenger or only nonregenerative extracellular

messenger [Fig. 1(C4), (C2)]. A sustained glutamate input ( $k_i$ ) was used as a stimulus in both simplified and realistic geometries. For quantification, the values of  $[\text{Ca}_i^{2+}]$  and  $[\text{IP}_3]$  in the center of cell ( $\star$  in Fig. 2) were calibrated in the realistic geometry, while the average values of  $[\text{Ca}_i^{2+}]$  and  $\text{IP}_3$  in cells were computed for the simplified geometry.

Figure 3(e) *in vivo* indicates that as the  $[\text{IP}_3]$  level decreases from the stimulated cell  $C(0)$  to remote cells, the  $\text{Ca}_i^{2+}$  response patterns evolve from transient with plateau at  $C(0)$  to oscillations at  $C(9)$  and to baseline spiking at  $C(10)$ , as reported in Ref. 67. Results for the model of an *in vitro* astrocytic network are similar, except that the amplitude of  $[\text{IP}_3]$  is about half of that of *in vivo* model, because there are more gap junctions present in the *in vivo* model than in the *in vitro* model (Fig. 2).

Figures 3(c) and 3(d) can be understood in the same context in terms of  $[\text{IP}_3]$ . In the interconnected rat hepatocytes [Fig. 3(c)], there was almost no transition in  $\text{Ca}_i^{2+}$  response patterns from one cell to another, implying that the  $[\text{IP}_3]$  levels in each cell are in a similar range or at least over some effective dosage ( $\sim 0.1 \mu\text{M}$ ) while quite different  $[\text{IP}_3]$  levels are expected when the intermediate cell is excised and  $\text{IP}_3$  diffusion is absent. The decrease level of  $[\text{IP}_3]$  available in the third cell implies the transition from high to low frequency baseline spiking.<sup>67</sup> The longer delay in the initial  $\text{Ca}_i^{2+}$  spikes in Fig. 3(d) was also reproducible in both *in vivo* and *in vitro* model when gap junctional permeability

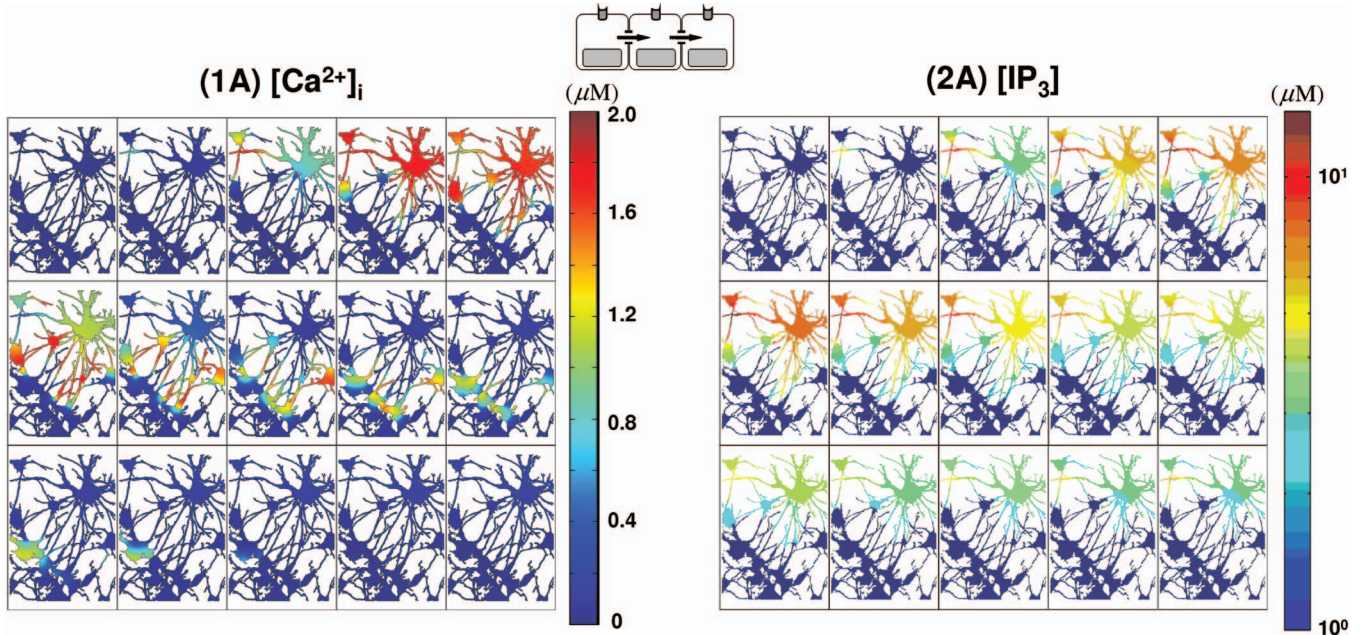


FIG. 4. (Color) Intracellular-messenger-mediated  $\text{Ca}_i^{2+}$  waves in a realistic network. (1A)  $\text{Ca}_i^{2+}$  waves by a glutamate stimulus in C(0) and mediated only by  $\text{IP}_3$  diffusion are shown on a linear scale. (2A) The corresponding  $\text{IP}_3$  waves plotted on a log scale. The temporal sequence of images in (1A) and (2A) runs from left to right and top to bottom. The elapsed time between images in (1A) and (2A) is  $\Delta t=0.2$  s with a total time of 3 s ( $t=0, 0.2, 0.4, \dots, 2.8, 3$ ).

( $k_{\text{perm}} \rho$ ) was set to zero, although the delay was more evident in the latter model [Figs. 3(e) and 3(f)].

## B. Gap junction mediated versus P2YR mediated $\text{Ca}_i^{2+}$ waves

In the absence of extracellular signaling, the distance that an initial calcium spike spreads depends on  $\text{IP}_3$  diffusion. The threshold value of  $\text{IP}_3$  for initiating a  $\text{Ca}_i^{2+}$  spike is  $\sim 0.1 \mu\text{M}$  (Figs. 4–6, Table II) and  $[\text{IP}_3]$  decreases rapidly from one cell to the next as  $\text{IP}_3$  diffuses through astrocytic gap junctions [Figs. 4(2A), 5(2A), and 6(2A), Table III]. As a result, the amplitudes of spikes along the spreading  $\text{Ca}_i^{2+}$  wave decrease rapidly and the wave dies within  $\sim 58.2 \mu\text{m}$  from C(0) [C(6), C(7), and C(10) in Fig. 4(1A), Table II] in the realistic geometry, whereas it vanishes in the fourth cell in the simplified geometry [Fig. 6(1A)]. Also, the velocity of  $\text{Ca}_i^{2+}$  waves decreases as shown in Figs. 5(1A) and 6(1A) and Table II.

On the other hand, when  $\text{Ca}_i^{2+}$  waves are mediated by nonregenerative ATP diffusion,  $[\text{IP}_3]$  decreases more slowly than when the waves are mediated by  $\text{IP}_3$  diffusion through gap junctions [Figs. 5(2B), 6(2B), and 7(2B), Table II]. Although the  $\text{Ca}_i^{2+}$  waves died after a few cells [Figs. 5(1B) and 6(1B), Table II] similar to the case of gap junction mediated  $\text{Ca}_i^{2+}$  waves, the amplitudes of initial spikes and the propagation velocity along  $\text{Ca}_i^{2+}$  wave remained constant [Figs. 5(1B) and 6(1B), Table II].

The effective dosage of ATP to trigger  $\text{Ca}_i^{2+}$  spike in the model was  $3 \mu\text{M}$  [Figs. 5(3B) and 6(3B), Table II], which is similar to the value reported in the literature.<sup>82,64</sup> The velocity as measured by the spread of the peak of nonregenerative ATP wave spread was  $\sim 50 \mu\text{m/s}$  in the realistic geometry

[Fig. 5(3B), Table II] and  $\sim 40 \mu\text{m/s}$  in the simplified geometry [4 cells in 1.5 s, Fig. 6(3B)], which is similar to reported values ( $41 \mu\text{m/s}$ ; Ref. 82).

Another noticeable feature of  $\text{Ca}_i^{2+}$  waves by mediated by  $\text{IP}_3$  diffusion is that there is very little delay in propagation between cells [Figs. 5(1A) and 6(1A), Table II], while  $\text{Ca}_i^{2+}$  waves by ATP signal show a longer delay time for propagation from one cell to the next [Figs. 5(1B) and 6(1B), Table II]. Although the diffusion coefficient of ATP is larger than that of  $\text{IP}_3$  (Table I), the results in Figs. 5(1A), 5(2A), 6(1A), and 6(2A) illustrate the higher velocity of gap junction mediated  $\text{Ca}_i^{2+}$  waves compared to P2YR mediated waves. This difference stems from the fact that  $\text{IP}_3$  is the critical species for initiating  $\text{Ca}_i^{2+}$  release, and when it spreads via gap junction there is little delay in initiating  $\text{Ca}_i^{2+}$  release, whereas additional time for  $\text{IP}_3$  production is required for ATP signaling by P2YR. Because of this delay, P2YR mediated  $\text{Ca}_i^{2+}$  waves are expected to be slower than gap junction mediated waves, and this is borne out by the measured speeds:  $\sim 15 \mu\text{m/s}$  [Figs. 5(1B) and 6(1B), Table II] versus  $40 \mu\text{m/s}$  [Figs. 5(1A) and 6(1A), Table II] in both simplified and realistic geometries. These also compare favorably to the experimentally observed ranges ( $15\text{--}27 \mu\text{m}^2/\text{s}$ ; Refs. 15, 18, 82, 113, and 120). It has also been reported that in  $\text{Ca}_i^{2+}$  wave propagation from Muller cells into astrocytes, there was a considerable delay,  $2.6 \pm 0.2$  s, while there was a shorter delay (0.85 s) in the case of wave spread from astrocyte processes to an adjacent Muller cell endfoot.<sup>82</sup> Other studies demonstrated a longer delay (5–10 s) in  $\text{Ca}_i^{2+}$  waves between different layers of cells in a hippocampal slice.<sup>57</sup> In the model, the delay times range between 0.4 and 1.6 s [Figs. 5(1B) and 6(1B), Table II].



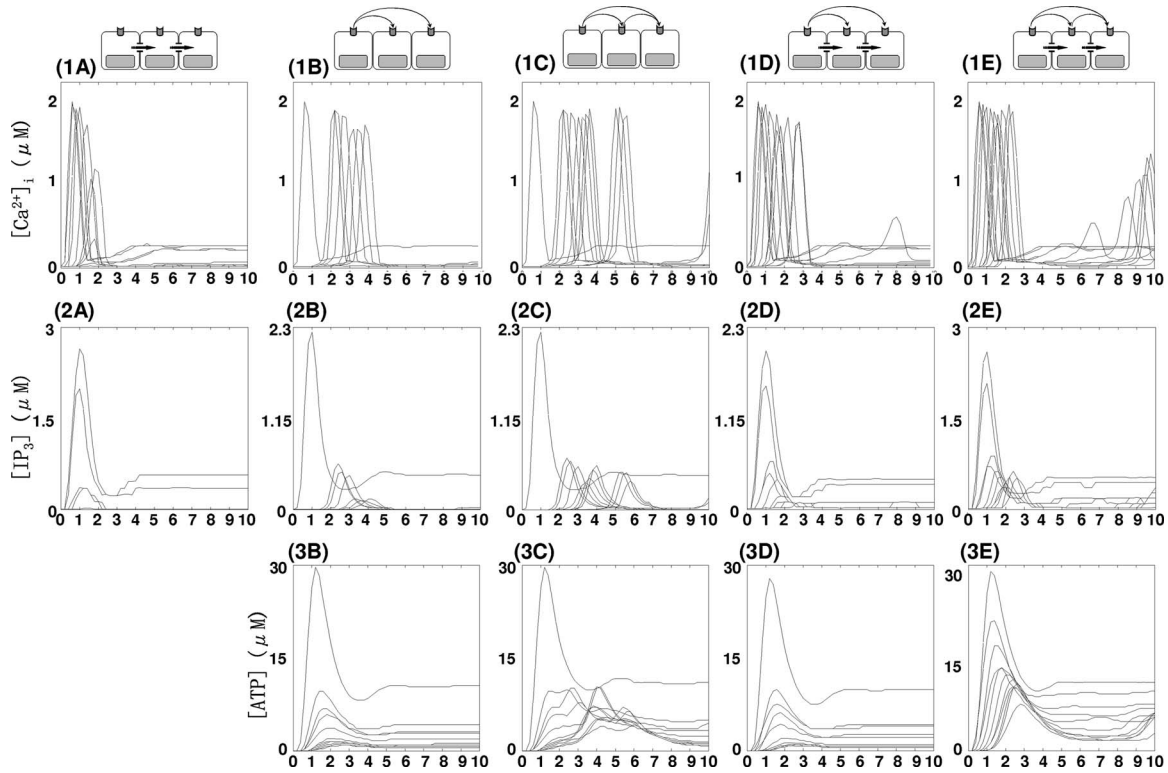


FIG. 5. A composite summary of the  $\text{Ca}_i^{2+}$  waves in the realistic cell network.  $\text{Ca}_i^{2+}$ ,  $[\text{IP}_3]$ , and  $[\text{ATP}]$  in  $C(i)$  were measured at the locations marked as  $\star$  in Fig. 2. The locations of the measuring point in descending order are C(2), C(9), C(1), C(3), C(4), C(8), C(5), C(10), C(7), and C(6) with distances from C(0) of 20.3, 29.8, 40.4, 42.4, 46.4, 49.3, 50.3, 58.2, 59.3, and 64.76 ( $\mu\text{m}$ ). In (1A), the traces whose peaks are above  $0.5 \mu\text{M}$  correspond to C(0), C(1), C(3), C(2), C(9), C(8), and C(4) from left to right, while the traces whose peaks are below  $0.5 \mu\text{M}$  correspond to C(5) and C(7) from top to bottom. In (2A), the traces from top to bottom represent  $[\text{IP}_3]$  in C(1), C(0), C(3), C(2), and C(10). In (1B), (1C), (2B), and (2C), the traces are of C(0), C(2), C(9), C(1), C(5), C(8), C(4), C(3), C(7), C(6), and C(10), while in distal order of C(0)-C(2)-C(9)-C(1)-C(5)-C(8)-C(4)-C(3)-C(7)-C(6)-C(10) from left to right traces in (3B) and (3C). In (1D) and (1E), the traces from left to right are  $\text{Ca}_i^{2+}$  from C(0), C(1), C(3), C(2), C(9), C(4), C(8), C(5), C(7), C(6) and C(10), whereas C(1)-C(0)-C(2)-C(3)-C(9)-C(4)-C(8)-C(7)-C(10) in (2D) and C(1)-C(0)-C(3)-C(2)-C(9)-C(4)-C(5)-C(8)-C(7)-C(6)-C(10) in (2E) from left to right, C(0)-C(2)-C(1)-C(9)-C(3)-C(4)-C(8)-C(10)-C(7)-C(6) in (3D) and C(0)-C(1)-C(2)-C(3)-C(9)-C(4)-C(5)-C(8)-C(7)-C(6)-C(10) in (3E).

Another difference between P2YR and gap junction mediated  $\text{Ca}_i^{2+}$  waves *in vivo* is reflected in the local  $[\text{IP}_3]$  concentration. Local  $[\text{IP}_3]$  can be larger than  $10 \mu\text{M}$  [Figs. 4(2A), 8(2D), and 8(2E)] for the *in vivo* gap junction mediated  $\text{Ca}_i^{2+}$  waves due to more “focused” diffusion along fine astrocytic processes. In contrast, the maximum  $[\text{IP}_3]$  remains less than  $3 \mu\text{M}$  for P2YR mediated waves [Figs. 7(2B) and 7(2C)]. On the other hand, in the simplified model which has more open connectivity in gap junctions,  $\text{IP}_3$  concentrations are less than  $3 \mu\text{M}$  in all cases, which is probably due to large gap junctional boundaries between cells (Fig. 6). A more detailed discussion on gap junctional connectivity and  $\text{Ca}_i^{2+}$  wave patterns can be found in Ref. 36.

### C. The effects of regenerative ATP signaling

Another contentious issue in  $\text{Ca}_i^{2+}$  signaling is whether or not ATP signaling is regenerative.<sup>37</sup> To see how the regenerative of ATP release affects the  $\text{Ca}_i^{2+}$  waves, Eqs. (2)–(6) were solved either for  $k_{\text{ATP}}=0$  or  $0.184/\text{s}$ . The velocities of initial  $\text{Ca}_i^{2+}$  spikes under the two scenarios were not distinguishable, even though the distance of  $\text{Ca}_i^{2+}$  wave spread was larger for regenerative ATP [(1B) and (1C) in Figs. 5–7, Table II]. Other differences can be seen from the ATP and  $\text{IP}_3$  profiles. When ATP release is assumed to be nonregenerative, peaks of  $[\text{ATP}]$  transients quickly decrease due to enzy-

matic degradation, whereas the summation of regenerative ATP release from each cell and diffusive spread from neighboring cells gives rise to steady amplitude of  $[\text{ATP}]$  transients in the regenerative case [Figs. 5(3B), 5(3C), 6(3B), and 6(3C)]. Although the waves travel further in the regenerative case, the ATP wave speed in both cases was  $\sim 40\text{--}50 \mu\text{m}/\text{s}$  [measured by the initial spikes in Figs. 5(3B), 5(3C), 6(3B), and 6(3C)].

Similar to what is observed for ATP wave propagation, in both cases the  $\text{Ca}_i^{2+}$  and  $\text{IP}_3$  wave velocities are similar at  $\sim 40 \mu\text{m}/\text{s}$  [(1B), (1C), (2B), and (2C) in Figs. 5 and 6]. The peak  $\text{IP}_3$  amplitude of the stimulated cell is unchanged at  $2.3 \mu\text{M}$  but the peak  $\text{IP}_3$  amplitudes of other cells diminish as a function of distance for nonregenerative ATP signaling, while they remain constant from the second cell on in the regenerative case due to ATP-stimulated  $\text{IP}_3$  downstream of the stimulated cell [Figs. 5(2B), 5(2C), 6(2B), and 6(2C)]. Also, a slight decrease in the amplitude of  $\text{Ca}_i^{2+}$  transients was observed in the nonregenerative ATP mediated  $\text{Ca}_i^{2+}$  wave, but the amplitude of  $\text{Ca}_i^{2+}$  transients remains constant in the regenerative ATP mediated  $\text{Ca}_i^{2+}$  waves [Figs. 5(1B), 5(1C), 6(1B), and 6(1C)].

Given the variety of calcium responses including oscillations that exist in a single cell,<sup>67</sup> it is worthwhile to understand why there is no sustained wave propagation in a net-

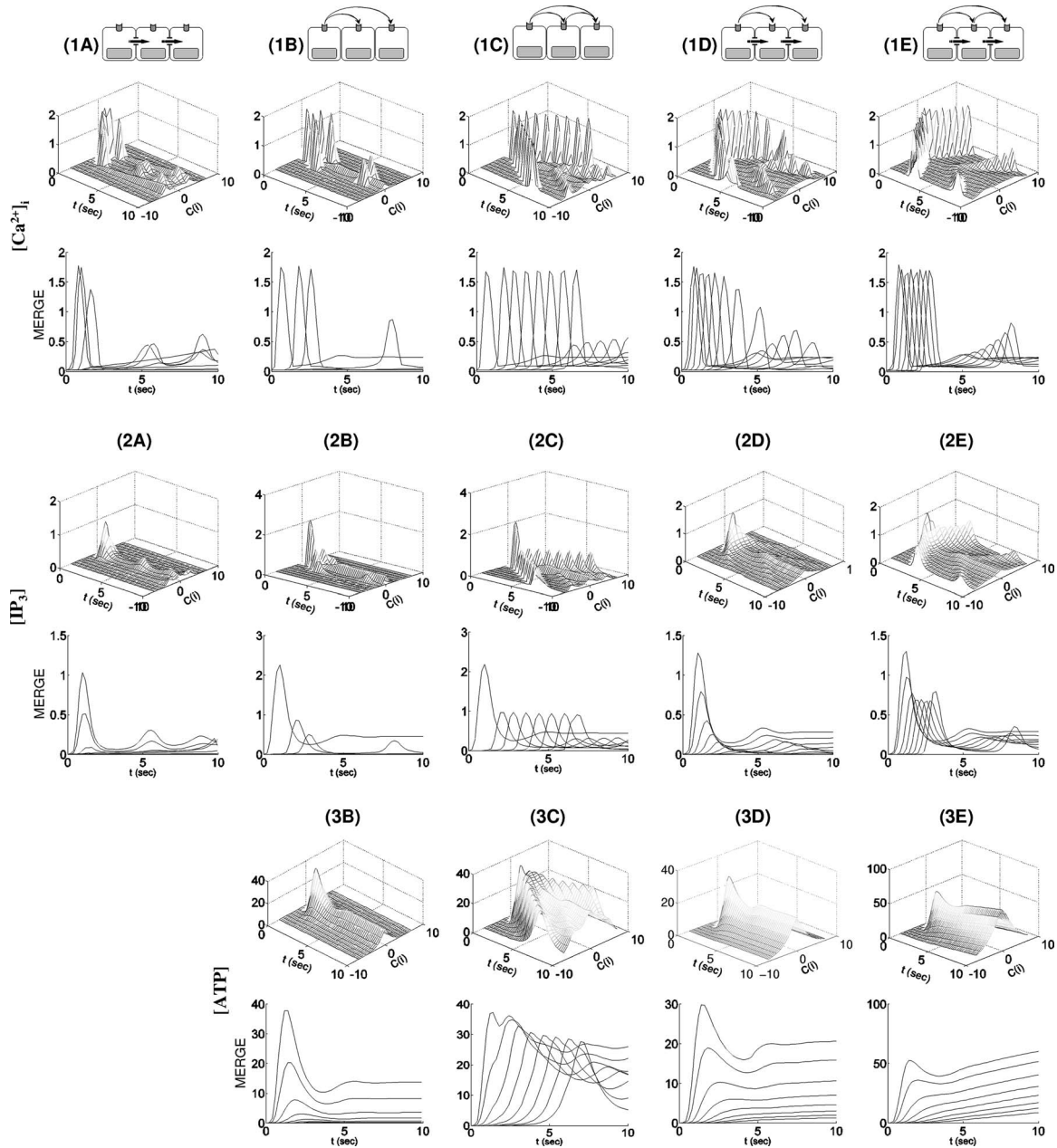


FIG. 6.  $\text{Ca}_i^{2+}$  waves in the simplified cell geometry. In the upper panels for  $\text{Ca}_i^{2+}$ ,  $[\text{IP}_3]$ , and  $[\text{ATP}]$ , the  $x$ - and  $y$ -axes represent time in seconds and the location of cells  $C(i)$  for  $i = 1, \dots, 10$ , respectively. On the  $z$ -axis is shown the average of the quantity over the cell (i.e., the integral of the quantity divided by the cell volume) plotted in increments of  $t=0.2$ . The lower panels (MERGE) showed the projected traces from the upper panels onto the  $y=0$  plane.

work. To this end we tested the linear stability of the steady state solution of Eq. (1) assuming zero gap-junctional permeability, which is equivalent to assuming that  $\text{Ca}_i^{2+}$  waves are mediated solely by ATP. The analysis of Eq. (1) shows that below the effective ATP dosage for  $\text{Ca}_i^{2+}$  response, all the real parts of the eigenvalues of Eq. (1) linearized about the steady state solution are negative, which prevents initiation of the  $\text{Ca}_i^{2+}$  response. Therefore, without regenerative ATP release the level of ATP that reaches the neighboring cells eventually drops below the effective ATP dosage as a result of diffusive spreading and enzymatic degradation (see Appendix C for details), and sustained propagation of  $\text{Ca}_i^{2+}$  waves is precluded. Furthermore, we have not found conditions that lead to propagation even if regenerative release is included.

#### D. Synergy of intra- and extracellular messengers

Thus far we have investigated the properties of  $\text{Ca}_i^{2+}$  response patterns initiated by either  $\text{IP}_3$  or ATP alone. Now we consider cases when both intra- and nonregenerative extracellular messengers carry  $\text{Ca}_i^{2+}$  release signals. Because we assume nonregenerative ATP signaling, the intracellular dynamics other than in  $C(0)$  do not influence ATP evolution [Figs. 7(3B) and 8(3D)].

Recall that the time scale of direct  $\text{IP}_3$  diffusion is faster than  $\text{IP}_3$  generation via ATP signaling [Figs. 5(2A), 5(2B), 6(2A), and 6(2B)]. When both  $\text{IP}_3$  and ATP are used for  $\text{Ca}_i^{2+}$  mobilization,  $\text{IP}_3$  diffusion dominates  $\text{Ca}_i^{2+}$  wave initiation as far as the  $\text{IP}_3$  concentration is above the effective threshold ( $\sim 0.1 \mu\text{M}$ ). Beyond that distance the generation of  $\text{IP}_3$  via

TABLE II. The characteristics of  $Ca_i^{2+}$  waves mediated by  $IP_3$  and/or ATP *in vivo* model.

		(A)	(B)	(C)	(D)	(E)
(1) $[Ca^{2+}]_i$	velocity ( $\mu\text{m/s}$ )					
	delay (sec)					
	amplitude ( $\mu\text{M}$ )					
	distance ( $\mu\text{m}$ )	$C(0) \sim C(5)$ $50.3 \mu\text{m}$	$C(0) \sim C(5)$ $50.3 \mu\text{m}$	$C(0) \sim C(11)$ $> 64.7 \mu\text{m}$	$C(0) \sim C(11)$ $> 64.7 \mu\text{m}$	$C(0) \sim C(11)$ $> 64.7 \mu\text{m}$
(2) $[IP_3]$	velocity ( $\mu\text{m/s}$ )					
	delay (sec)					
	amplitude ( $\mu\text{M}$ )					
	distance ( $\mu\text{m}$ )	$C(0) \sim C(5)$ $50.3 \mu\text{m}$	$C(0) \sim C(5)$ $50.3 \mu\text{m}$	$C(0) \sim C(11)$ $> 64.7 \mu\text{m}$	$C(0) \sim C(11)$ $> 64.7 \mu\text{m}$	$C(0) \sim C(11)$ $> 64.7 \mu\text{m}$
(3) [ATP]	velocity ( $\mu\text{m/s}$ )	N/A				
	delay (sec)	N/A				
	amplitude ( $\mu\text{M}$ )	N/A				
	distance ( $\mu\text{m}$ )	N/A	$C(0) \sim C(5)$ $50.3 \mu\text{m}$	$C(0) \sim C(11)$ $> 64.7 \mu\text{m}$	$C(0) \sim C(11)$ $> 64.7 \mu\text{m}$	$C(0) \sim C(11)$ $> 64.7 \mu\text{m}$
0: $C(0)$ , 1 <sup>st</sup> Column ; [ $C(2)$ , $C(9)$ , $C(1)$ ] , 2 <sup>nd</sup> column: [ $C(3)$ , $C(4)$ , $C(8)$ , $C(5)$ , $C(10)$ ], 3 <sup>rd</sup> column: [ $C(7)$ , $C(6)$ ]						

the ATP pathway serves to elevate  $IP_3$  above the threshold. Therefore, in short range  $Ca_i^{2+}$  wave propagation by pure  $IP_3$  diffusion is dominant, while  $Ca_i^{2+}$  wave propagation by ATP signaling is dominant in cells distant from the stimulation point [(1A), (1B), and (1D) in Figs. 5 and 6]. As the result, longer delay in  $Ca_i^{2+}$  wave propagation is observed for re-

mote cell locations, in contrast with rapid continuous wave propagation near the stimulated cell [Figs. 5(1D) and 6(1D)].

Another consequence of synergy between intra- and extracellular messengers is the propagation distance. While either an ATP signal without  $IP_3$  diffusion or  $IP_3$  diffusion without an ATP signal results in decaying waves, the syner-

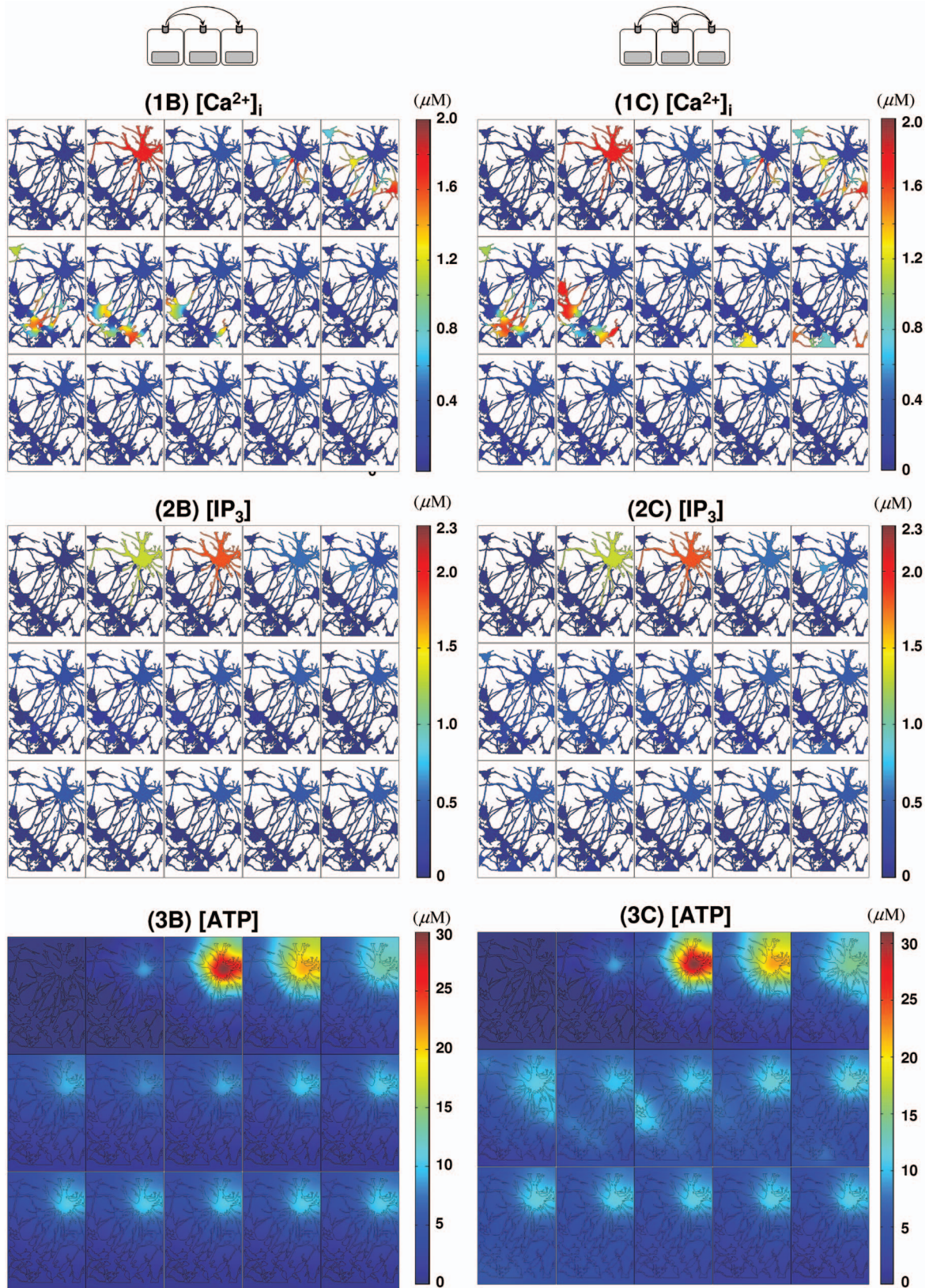


FIG. 7. (Color) Extracellular messenger mediated  $\text{Ca}_i^{2+}$  waves.  $\text{Ca}_i^{2+}$  waves initiated by a glutamate stimulus in C(0) and mediated only by ATP are shown. In (1B)–(3B), excitation is mediated by nonregenerative ATP spread, while regenerative ATP release is present in (1C)–(3C). The images in each panel [(1B)–(3B) and (1C)–(3C)] run from left to right and top to bottom. In each panel, the time elapsed between images is  $\Delta t=0.6$  s with total time of 8.4 s ( $t=0, 0.6, 1.2, \dots, 7.8, 8.4$ ).

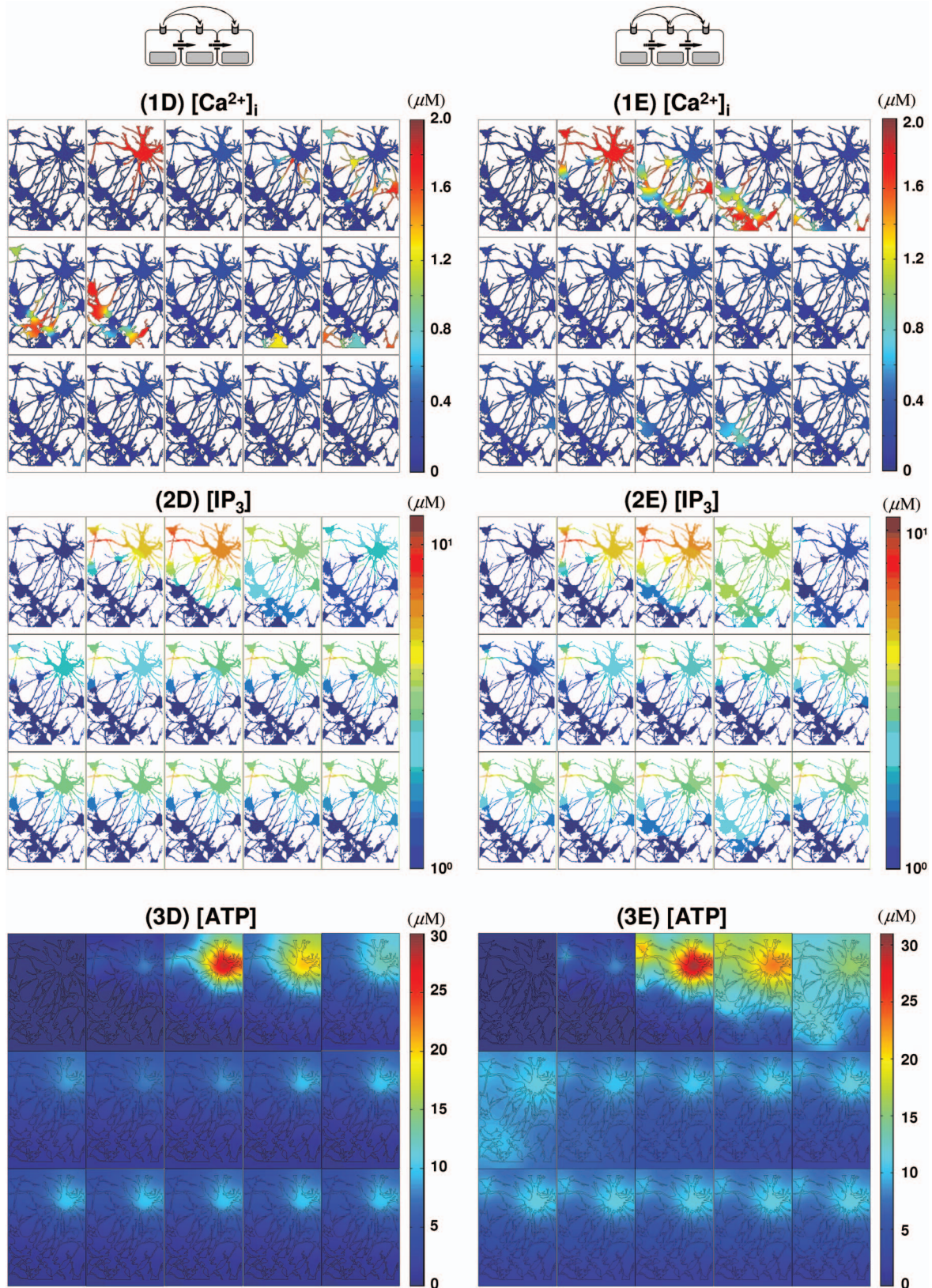


FIG. 8. (Color) Extracellular volume and  $Ca^{2+}$  wave by regenerative extracellular messenger

gistic activity of the two pathways gives rise to permanent waves that propagate through the entire computational domain, as shown in Figs. 4, 7, and 9. More quantitatively, (1A) and (2A) in Figs. 5 and 6 indicate that no  $Ca^{2+}$  re-

sponses were found in the distant cells [ $C(i), i=6, 7, 10$  in the realistic geometry and  $i \geq 4$  in the simplified geometry] when either intra- or extracellular messenger was applied independently. However, when both intra- and extracellular

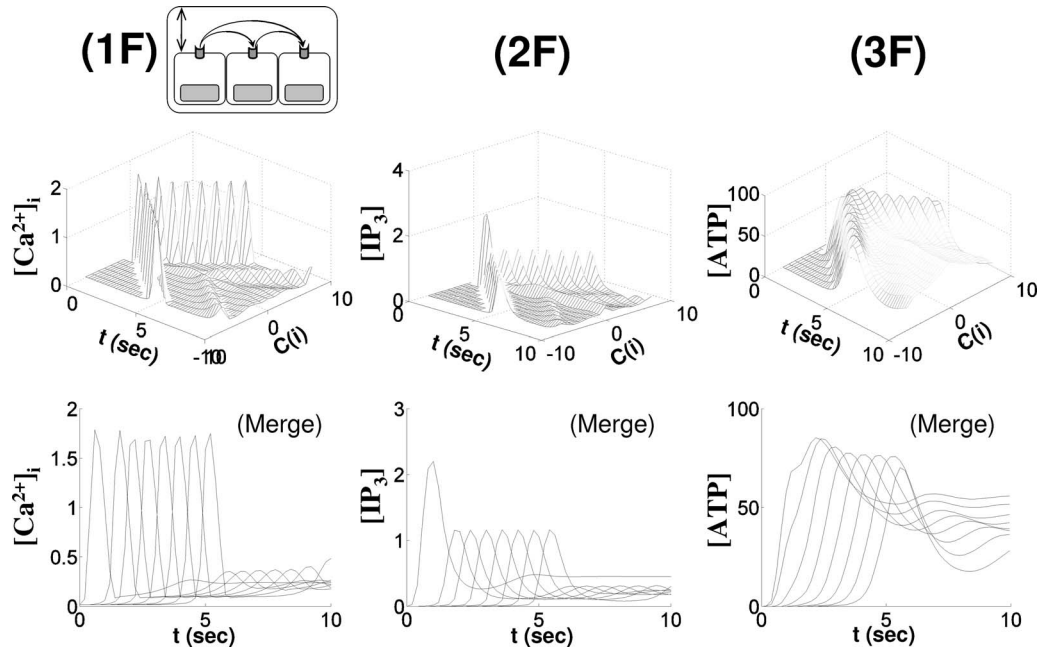


FIG. 9. The synergy between intra- and extracellular messengers in  $\text{Ca}_i^{2+}$  waves.  $\text{Ca}_i^{2+}$  waves initiated by glutamate in  $C(0)$  and mediated by both ATP and  $\text{IP}_3$  are shown. In (1D)–(3D) are shown  $\text{Ca}_i^{2+}$  waves mediated by nonregenerative ATP spread, while regenerative ATP release is present in (1E)–(3E). The color maps for  $\text{Ca}_i^{2+}$  and ATP are on a linear scale [(1D), (3D), (1E), and (3E)], while  $\text{IP}_3$  [(2D) and (2E)] is scaled logarithmically. The images in each panel [(1D)–(3D), (1E)–(3E)] are read from left to right and top to bottom and the time elapsed between images in each panel is  $\Delta t = 0.6$  s with total time of 8.4 s ( $t = 0, 0.6, 1.2, \dots, 7.8, 8.4$ ).

messengers are present,  $\text{Ca}_i^{2+}$  transients are observed in all cells [Figs. 5(1D) and 6(1D), Table II]. This indicates that when both  $\text{IP}_3$  and ATP are used for  $\text{Ca}_i^{2+}$  mobilization, the fast  $\text{IP}_3$  diffusion can either mobilize  $\text{Ca}_i^{2+}$  or sensitize cells by eliciting a subthreshold  $\text{Ca}_i^{2+}$  responses. After additional  $\text{IP}_3$  is received via the slower process of  $\text{IP}_3$  production by ATP, the  $\text{IP}_3$  level in sensitized cells reaches the threshold level ( $\sim 0.1 \mu\text{M}$ ) and  $\text{Ca}_i^{2+}$  transients are induced. As shown in (1B) and (2D) in Figs. 5 and 6, a slight decrease in the amplitude of  $\text{Ca}_i^{2+}$  transients was observed in the nonregenerative ATP mediated  $\text{Ca}_i^{2+}$  wave, while a constant amplitude of  $\text{Ca}_i^{2+}$  transients was observed in the regenerative ATP-mediated waves [Figs. 5(1C) and 6(1C)]. A similar observation can be made concerning ATP-mediated waves even with  $\text{IP}_3$  diffusion through gap junctions. Moreover, regenerative ATP-mediated waves propagate like true traveling wave patterns, retaining the initial  $\text{Ca}_i^{2+}$  spike profile along the  $\text{Ca}_i^{2+}$  wave [Figs. 5(1C), 5(1E), 6(1C), and 6(1E)].

Another interesting result is that when  $\text{IP}_3$  diffusion is included in the realistic geometry, a second wave was initiated from  $C(4)$  to  $C(9)$  which died out beyond  $C(9)$  [Figs. 5(1E) and 8(1E)]. In this case,  $C(2)$  shows a transient with plateau type of  $\text{Ca}_i^{2+}$  response pattern similar to that  $C(0)$  and  $C(1)$ , while the cells  $C(4) \cdots C(9)$  show an oscillatory  $\text{Ca}_i^{2+}$  response pattern. Apparently the signal transferred from  $C(9)$  to its downstream neighbors was not strong enough to elevate  $\text{IP}_3$  above threshold for wave initiation, but even so, the signal from  $C(9)$  integrated the signal relayed from  $C(4)$  and could, in living cells, influence the future response of these downstream cells [Figs. 5(1E) and 8(1E)].

In both the simplified and realistic geometries, the ATP wave propagation pattern indicates that for regenerative ATP

without  $\text{IP}_3$  diffusion, the peak amplitude of ATP was lower than for regenerative ATP with  $\text{IP}_3$  diffusion [Figs. 5(3C), 5(3E), 6(3C), and 6(3E)]. Also, the maximum point of ATP spread from  $C(0)$  can be easily identified in Figs. 5(3C) and 6(3C), while when there is regenerative ATP with  $\text{IP}_3$  diffusion, the extracellular effect of ATP released from a cell cannot be clearly identified [Figs. 5(3E) and 6(3E)]. Also, accumulation of ATP was observed in the simplified geometry due to the ATP released into the restricted extracellular space, something that is not observed in the sparsely distributed cells in the realistic geometry [Figs. 5(3E) and 6(3E)]. This may also explain why extracellular ATP is believed to be a major contributor to  $\text{Ca}_i^{2+}$  waves in cultured astrocytes.<sup>54,58,11,53,63</sup>

### E. The role of the extracellular volume

In reality the extracellular space in the brain provides a tortuous path for molecular diffusion, and it is important to understand how the extracellular volume influences ATP signaling. For this purpose, the volume of the extracellular space was modified via an extracellular volume dependent parameter  $\gamma = 1/L$ , where  $L$  is the thickness of the extracellular space (Appendix B). Here  $\gamma$  was chosen as  $1.087 \mu\text{m}^{-1}$ , but because the ATP concentration in a cell is high ( $30 \mu\text{M}$ ), any change in  $L$  could result in a large change in ATP dynamics. To take this factor into account, we redid some computations in the case of regenerative ATP signaling using  $\frac{1}{2}L = 2\gamma$ , which in effect doubles the source term  $\gamma k_{\text{ATP}} \phi(P)(A_T - A)$  in Eq. (6).

In comparison with Fig. 6(3C), the peak amplitude of ATP was doubled (from 38 to 85  $\mu\text{M}$ ), and the propagation

of ATP waves showed similar traveling wavelike patterns (Fig. 8). However, the average ATP and IP<sub>3</sub> wave velocity increased from 24.49 [Fig. 6(3C)] to 34.29  $\mu\text{m/s}$  [Fig. 8(3F)]. The IP<sub>3</sub> profiles were not distinguishable between the two cases having similar amplitudes [Fig. 6(3C) and Fig. 8(3F)]. Similarly, Ca<sub>i</sub><sup>2+</sup> wave velocity increased from 24.00 to 26.09  $\mu\text{m/s}$  with constant amplitudes and the delay between cells was shortened [Fig. 6(3C) and Fig. 8(3F)]. Although the extracellular volume strongly influences the ATP dynamics, the effects on intracellular amplitudes of Ca<sub>i</sub><sup>2+</sup> and IP<sub>3</sub> were minimal [Figs. 6(1C), 6(2C), 8(1F), and 8(2F)]. Thus the primary effect of the higher ATP signal is to speed up wave initiation and propagation.

In light of the nonuniform and complex spatial distribution of cells and extracellular space in the brain, these results imply that Ca<sub>i</sub><sup>2+</sup> wave patterns can be very complex with a wide range of speeds and response times. Especially, when regenerative ATP is involved, the local maximal ATP that defines local Ca<sub>i</sub><sup>2+</sup> wave velocity and delay time between cells was proportional to  $\gamma$ , and amplification and dilution of the strength of extracellular signaling could be accomplished by modifying the extracellular geometry. There is evidence that astrocytes have the ability to control the extracellular volume by gating VRACs and swelling in K<sup>+</sup> ion concentration and ATP dependent manner, even though the underlying mechanism has not been fully understood.<sup>106,87,75,71,77</sup> Therefore, ATP may have more complex, indirect, self-regulatory roles in diffusion by modulating volume-sensitive anion channels, which in turn affects ATP diffusion.

#### IV. CONCLUSIONS

It is widely believed that both direct coupling via the intracellular messenger IP<sub>3</sub> and indirect coupling via the extracellular messenger ATP are involved in cell-cell signaling in astrocyte networks, but the relative importance of each mode has not been established in general. The model developed herein, which utilizes a detailed model of signal transduction and intracellular calcium dynamics for single cells developed earlier,<sup>67</sup> allows for both modes of transport in both simplified and realistic network topologies. Simulations of the model in simplified and realistic geometries demonstrated that Ca<sub>i</sub><sup>2+</sup> waves induced by individual messengers have distinct characteristics of propagation speed, propagation distance, delay between cells, and Ca<sub>i</sub><sup>2+</sup> transient profiles. It was also found that synergistic effects of intracellular IP<sub>3</sub> and extracellular ATP on Ca<sub>i</sub><sup>2+</sup> waves can be very complex, but the model developed here can be used to explore these effects.

While the IP<sub>3</sub>-mediated Ca<sub>i</sub><sup>2+</sup> waves propagate rapidly with at most a short delay between cells, they only propagate for a few cells and the corresponding amplitude of Ca<sub>i</sub><sup>2+</sup> transients decreases significantly from cell to cell. Similar effects are observed for ATP-mediated waves, but the delay time in Ca<sub>i</sub><sup>2+</sup> waves between cells is much longer for reasons adduced earlier, which leads to slower Ca<sub>i</sub><sup>2+</sup> wave propagation and slower decay of Ca<sub>i</sub><sup>2+</sup> transients.

Ca<sub>i</sub><sup>2+</sup> waves mediated by both IP<sub>3</sub> and ATP display a mix of all the characteristics of the separate cases. While there is little or no delay in the Ca<sub>i</sub><sup>2+</sup> wave close to stimulated cell,

longer delays were observed in the remote cells. Overall decay of Ca<sub>i</sub><sup>2+</sup> wave front transients was similar to that of ATP mediated Ca<sub>i</sub><sup>2+</sup> wave, and Ca<sub>i</sub><sup>2+</sup> wave propagation reached all the cells in the domain of consideration.

When regenerative ATP release was considered, the Ca<sub>i</sub><sup>2+</sup> waves display a more permanent form and propagate at a constant speed, regardless of whether or not IP<sub>3</sub> served as a messenger. However, the wave speed was much larger when both IP<sub>3</sub> and regenerative ATP were involved [Fig. 7(1C), (1E)]. The characteristics of Ca<sub>i</sub><sup>2+</sup> waves in this case are summarized in Table II. One clear conclusion is that regenerative release of ATP can lead to long distance propagation in networks.

While the qualitative behaviors of Ca<sub>i</sub><sup>2+</sup> responses are independent of the geometries considered, IP<sub>3</sub> kinetics strongly depend on the geometries especially on the gap junctional connectivity among the astrocytes. When higher gap junctional connectivity was established through an astrocytic network, IP<sub>3</sub> easily diffuses out to neighboring cells, thereby controlling the [IP<sub>3</sub>] in cells. In contrast, the lower gap junctional connectivity observed in the realistic geometry of an astrocyte network leads to local [IP<sub>3</sub>] greater than 10  $\mu\text{M}$ .

Regenerative ATP-driven waves also show geometry dependence. When cell density in the astrocytic network is high as in the case of the simplified geometry, regenerative ATP alone can exceed the ATP decay rate and lead to local elevated concentrations for the parameters chosen. However, in the realistic geometry where there is a large area of cell free domains, the ATP released decays rapidly and the concentration remains close to the steady state level. Of course no geometry dependency in observed ATP is nonregenerative because the only ATP release is from the stimulated cell.

Experimentally observed Ca<sub>i</sub><sup>2+</sup> waves in astrocyte networks exhibit decaying speeds (from the site of initiation) in the range of 200  $\mu\text{m}$ ,<sup>15,113</sup> a maximal propagation range of 200–350  $\mu\text{m}$  in radius, and a maximal speed of 15–27  $\mu\text{m/s}$ .<sup>15,113,120,82,18</sup> Our results replicate the decaying amplitudes when Ca<sub>i</sub><sup>2+</sup> waves are mediated by either IP<sub>3</sub> or IP<sub>3</sub> and nonregenerative ATP, and the decrease in the velocity is observed in both cases. The maximal velocity in both cases is over 40  $\mu\text{m/s}$ , which is larger than the values reported in the literature. However, when IP<sub>3</sub> was the only messenger, the effective range of Ca<sub>i</sub><sup>2+</sup> waves was much lower than 200–350  $\mu\text{m}$ , while Ca<sub>i</sub><sup>2+</sup> waves propagate over 100  $\mu\text{m}$ . In contrast, when regenerative ATP release is involved the waves display a more permanent form, which has not been reported. From this we conclude that Ca<sub>i</sub><sup>2+</sup> waves in an astrocyte network are probably mediated by both intracellular IP<sub>3</sub> and nonregenerative extracellular ATP (or partially regenerative ATP as suggested in Ref. 74).

#### ACKNOWLEDGMENTS

This work was supported by NIH Grant GM 29123 (Hans G. Othmer) and NIH RO1 GM073846 (Anne K. Kenworthy).

## APPENDIX A: PHYSICAL INTERPRETATION OF SIMPLIFIED TEMPORAL MODEL

Examination of Eq. (1) indicates that each equation has a source term and a decay term. For example,

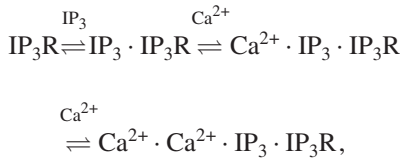
$$\frac{dP}{dt} = J_{\text{source}}^P - J_{\text{decay}}^P,$$

where  $J_{\text{source}} = k_1 C / (1 + k_2 K)$  and  $J_{\text{decay}} = k_3 P$ . Therefore IP<sub>3</sub> production by PLC ( $J_{\text{source}}$ ) is a function of cytosolic free Ca<sub>i</sub><sup>2+</sup> and PKC with property  $J_{\text{source}} \propto C$ ,  $1/K$  with dependence on some parameters  $k_1$  (s<sup>-1</sup>) and  $k_2$  (μM<sup>-1</sup>). Since  $K$  is positive and the denominator  $(1 + k_2 K) \geq 1$ , the expression shows explicit inhibition of PKC in IP<sub>3</sub> production. Likewise, the activation of PKC shows the relationships PKC  $\propto$  Ca<sub>i</sub><sup>2+</sup> and free PKC ( $K_0 - K$ ) and

$$\frac{dK}{dt} = J_{\text{activate}}^K - J_{\text{decay}}^K,$$

where  $J_{\text{activate}} = k_4 C (K_0 - K)$  and  $J_{\text{decay}} = -k_5 K$ . Here,  $k_4$  (μM<sup>-1</sup> s<sup>-1</sup>) is the rate constant for  $K$  and  $C$  binding and  $k_5$  is decay rate for  $K$ .

Although in  $R$ -kinetics, the source term is quite complicated comparing with previous two cases, we can apply similar argument. Previously, the Tang and Othmer<sup>107</sup> Ca<sup>2+</sup> model was implemented for IP<sub>3</sub> induced Ca<sup>2+</sup> release from the ER,



where  $R$  (Ca<sup>2+</sup> · Ca<sup>2+</sup> · IP<sub>3</sub> · IP<sub>3</sub>R)  $\propto$   $P$ ,  $C^2$ , and free IP<sub>3</sub>R. This leads us to

$$\frac{dR}{dt} = J_{\text{activate}}^R - J_{\text{decay}}^R$$

for activated state ( $J_{\text{activate}} \propto PC^2 \text{IP}_3\text{R}$ ) and decay ( $J_{\text{decay}} \propto R$ ) of  $R$ . Because we want an ODE system of  $P$ ,  $K$ ,  $R$ , and  $C$ , we followed the computation described in Refs. 107 and 66 to remove the dependency on free IP<sub>3</sub>R of  $J_{\text{activate}}$ . This step leads us to  $J_{\text{activate}}^R = k_6 PC^2 (R_T - R) / (1 + k_7 P (1 + k_8 C))$  and  $J_{\text{decay}}^R = k_9 R$  as desired, where  $k_6$  (μM<sup>-2</sup> s<sup>-1</sup>) is the binding rate constant for  $P$ ,  $C^2$ , and IP<sub>3</sub>R,  $k_9$  (s<sup>-1</sup>) is the offrate constant of  $R$ ,  $k_7$  (μM<sup>-1</sup>), and  $k_8$  (μM<sup>-1</sup>) are the affinity constant for (IP<sub>3</sub>, IP<sub>3</sub>R) and (Ca<sub>i</sub><sup>2+</sup>, IP<sub>3</sub> · IP<sub>3</sub>R).

Finally, the cytosolic Ca<sub>i</sub><sup>2+</sup> dynamics is governed by following equation:

$$\frac{dC}{dt} = J_{\text{leak}}^C + J_{\text{IP}_3}^C - J_{\text{SERCA}}^C,$$

where  $J_{\text{leak}}^C$  is the basal Ca<sub>i</sub><sup>2+</sup> release from ER,  $J_{\text{IP}_3}^C$  is the IP<sub>3</sub> induced Ca<sub>i</sub><sup>2+</sup> release, and  $J_{\text{SERCA}}^C$  is the clearance of Ca<sub>i</sub><sup>2+</sup> by SERCA pump on ER. If we let  $k_c$  (micromolar) be volume averaged Ca<sub>i</sub><sup>2+</sup> concentration in cytosol (i.e., the equilibrium of Ca<sub>i</sub><sup>2+</sup> levels the cytosolic Ca<sub>i</sub><sup>2+</sup> concentration approach when the whole ER network is ruptured), then

$$J_{\text{leak}} = k_{10}(k_c - C),$$

where  $k_{10}$  (s<sup>-1</sup>) is the basal Ca<sub>i</sub><sup>2+</sup> release rate. The IP<sub>3</sub> induced Ca<sub>i</sub><sup>2+</sup> release ( $J_{\text{IP}_3}^C$ ) is a function of  $(k_c - C)$  and Ca<sub>i</sub><sup>2+</sup> · IP<sub>3</sub> · IP<sub>3</sub>R (i.e.,  $J_{\text{IP}_3}^C \propto (k_c - C)[\text{Ca}^{2+} \cdot \text{IP}_3 \cdot \text{IP}_3\text{R}]$ ), but if we use the similar argument to express Ca<sub>i</sub><sup>2+</sup> · IP<sub>3</sub> · IP<sub>3</sub>R in term of  $R$  as we used in free IP<sub>3</sub>R (Refs. 107 and 66) to get

$$J_{\text{IP}_3}^C = \bar{k}_{11} \frac{\tilde{k}_{11} CP (R_T - R)}{1 + k_7 P (1 + k_8 C)} (k_c - C),$$

where  $\tilde{k}_{11}$  (μM<sup>-2</sup>) denotes affinity constant for  $C$ ,  $P$ , and free IP<sub>3</sub>R binding, and  $\bar{k}_{11}$  (μM<sup>-1</sup> sec<sup>-1</sup>) denotes Ca<sub>i</sub><sup>2+</sup> release rate from IP<sub>3</sub>R Ca<sup>2+</sup>Ca<sup>2+</sup> channels. If we define  $k_{11}$  (μM<sup>-3</sup>) =  $\bar{k}_{11} \tilde{k}_{11} / k_{10}$ , then we can combine  $J_{\text{leak}}^C$  and  $J_{\text{IP}_3}^C$  as  $J_{\text{source}}^C$ ,

$$J_{\text{source}}^C = J_{\text{leak}}^C + J_{\text{IP}_3}^C = k_{10} \left( 1 + \frac{k_{11} PC (R_T - R)}{1 + k_7 P (1 + k_8 C)} \right) (k_c - C).$$

Finally, we assume that  $J_{\text{SERCA}}$  follows the Hill-type kinetics with Hill coefficient two<sup>67</sup> so that

$$J_{\text{SERCA}} = \frac{k_{12} C^2}{C^2 + k_{p2}^2},$$

where  $k_{12}$  (μM s<sup>-1</sup>) and  $k_{p2}$  (μM) denote the maximal Ca<sup>2+</sup> pumping rate and Ca<sup>2+</sup> sensitivity of the SERCA pump, respectively.

## APPENDIX B: ATP KINETICS

Let the height of extracellular space at the location of ATP release be  $L$  and define  $M$  as total mass of ATP ( $A$ ) in the infinitesimal volume at the ATP release site (i.e.,  $M = AL \delta x \delta y$ ). From the conservation of mass and ATP decay by enzyme, the change in  $M$  over time is given by

$$\frac{\partial M}{\partial t} = \sum \dot{m}_{\text{in}} - \sum \dot{m}_{\text{out}} - \dot{m}_{\text{decay}}, \quad (\text{B1})$$

where  $\dot{m}_{\text{in}} = q_{x,\text{in}} \delta y L + q_{y,\text{in}} \delta x L + q_{z,\text{in}} \delta x \delta y$  and  $\dot{m}_{\text{out}} = q_{x,\text{out}} \delta y L + q_{y,\text{out}} \delta x L$  denote mass fluxes while  $\dot{m}_{\text{decay}} = k_{-\text{ATP}} M$  represents loss of mass due to decay.

Assuming Fick's law diffusion for the fluxes, applying a Taylor series expansion, and truncating, we obtain

$$\frac{\partial A}{\partial t} = -D_A \Delta A - \frac{1}{L} q_{z,\text{in}} - k_{-\text{ATP}} A, \quad (\text{B2})$$

which does not involve  $z$ .

If the extracellular space is assumed to be uniform in height  $L$ , the value of  $L$  is computed from the observation that body fluid is composed of 28.0 l of intracellular fluid and 14.0 l of extracellular fluid, which is again composed of 3.0 l plasma fluid and 11.0 l of interstitial fluid. From the ratio of interstitial and intracellular fluids of 11/28,<sup>55</sup> we have  $L = 0.4l$  (μm), where  $l$  is the thickness of cells. With a choice of  $l = 2.33$ , the cell thickness, we estimated  $L = 0.92$  μm (Table I, Fig. 2).

Because the ATP release mechanism is unknown, we assume that ATP release is proportional to the ATP concentration gradient between intra- and extracellular spaces in IP<sub>3</sub> dependent manner,



$$q_{z,\text{in}} = k_{\text{ATP}}\phi(P)(A_T - A),$$

where  $k_{\text{ATP}}(\text{s}^{-1})$  is the ATP release rate,  $\phi(P)$  is the  $\text{IP}_3$  dependence of ATP release, and  $A_T$  is the intracellular concentration of ATP. The dependence of ATP release on  $\text{IP}_3$  has been reported from some studies,<sup>19,20</sup> but the function  $\phi$  is unknown and we will choose  $\phi(P_1) = P_1/(\rho + P_1)$  in the current model. We will approximate  $k_{\text{ATP}}(\text{s}^{-1})$  so that the peak amplitude of ATP release is  $30 \mu\text{M}$ .

Putting this and Eq. (B2) together, we get

$$\frac{\partial A}{\partial t} = D_A \Delta A + \frac{1}{L} k_{\text{ATP}} f(P)(A_T - A) - k_{-\text{ATP}} A. \quad (\text{B3})$$

In summary, the ATP kinetics can be described domain-wise as the initial boundary value problem

$$\frac{\partial A}{\partial t} = \begin{cases} D_A \frac{\partial^2 A}{\partial x^2} + \gamma k_{\text{ATP}} f(P_1)(A_T - A) - k_{-\text{ATP}} A \\ \text{in } C(i)(0, \infty) \\ D_A \frac{\partial^2 A}{\partial x^2} + k_{-\text{ATP}} A \quad \text{in } \text{Ex}(0, \infty), \end{cases}$$

$$A(x, y, 0) = 0, \quad D_A \frac{\partial A}{\partial n} = -A \quad \text{on } \Omega,$$

where  $i=0, \dots, 10$  and  $\gamma=1/L$ . For nonregenerative ATP release, we set  $k_{\text{ATP}}=0$ .

### APPENDIX C: $\text{Ca}_i^{2+}$ WAVE PROPAGATION

Since we are interested in P2YR mediated  $\text{Ca}_i^{2+}$  waves, we assume that  $k_{\text{perm } p}=0$  in this section. A necessary condition for a  $\text{Ca}_i^{2+}$  wave initiated in one astrocyte to propagate to neighboring astrocytes is that  $[\text{IP}_3]$  in the neighboring astrocytes should be above the effective dosage for  $\text{Ca}_i^{2+}$  response. Our previous study<sup>67</sup> indicates that various  $\text{Ca}_i^{2+}$  responses may occur for  $[\text{IP}_3]$  above the effective dosage via a change in the linear stability of the steady state solution. If  $[\text{IP}_3]$  is not high enough then the steady state solution remains stable and there exists no  $\text{Ca}_i^{2+}$  response in the cell, i.e., a  $\text{Ca}_i^{2+}$  wave stops. In this sense,  $\text{Ca}_i^{2+}$  wave propagation in an astrocytic network is completely determined by the linear stability of the steady state solution to Eq. (1),

$$\begin{aligned} \frac{dR}{dt} &= \frac{k_6 P C^2 (R_T - R)}{1 + k_7 P (1 + k_8 C)} - k_9 R, \\ \frac{dC}{dt} &= k_{10} \left( 1 + \frac{k_{11} P C (R_T - R)}{1 + k_7 P (1 + k_8 C)} \right) (k_c - C) - \frac{k_{12} C^2}{C^2 + k_{p2}^2}, \end{aligned} \quad (\text{C1})$$

which was studied extensively in Ref. 107 for  $K=0$ . Let  $P = \bar{P}$ , which is above the effective dosage such that linearized Eq. (C1) at the steady state solution has a pair of complex conjugate eigenvalues. By a continuity argument applied to the eigenvalues, we can prove that there exists an open set around  $(\bar{P}, 0)$  where the linearized equation (C1) at the steady state solution has complex conjugate eigenvalues.

Next, If we write Eq. (1) as  $dX/dt = \Phi(X)$ , where  $X = (P, K, R, C)$ , the steady state solutions  $\bar{X} = (\bar{P}, \bar{K}, \bar{R}, \bar{C})$  of Eq. (1) are given by  $\Phi(\bar{X})=0$ . Linearizing about  $\bar{X}$ , we get

$$\frac{d(X - \bar{X})}{dt} = D\Phi(\bar{X})(X - \bar{X}), \quad (\text{C2})$$

and the linear stability of  $\bar{X}$  is determined by the eigenvalues  $\Lambda = (\mu_1, \mu_2, \lambda_1, \lambda_2)$  of the matrix  $D\Phi(\bar{X})$ . Because there exists an open set around  $(\bar{P}, 0)$  where linearized Eq. (C1) at the steady state solution has complex conjugate eigenvalues, if  $P$  and  $K$  dynamics are confined in the open set around  $(\bar{P}, 0)$ , Eq. (C2) also has complex conjugate eigenvalues. Indeed, we can find an invariant rectangular domain near  $(\bar{P}, 0)$  bounded by

$$P = \frac{k_1 \bar{C} (k_4 \bar{C} + k_5)}{k_3 (k_4 (k_2 K_T + 1) \bar{C} + k_5)} + \epsilon,$$

$$P = \frac{k_1 \bar{C} (k_4 \bar{C} + k_5)}{k_3 (k_4 (k_2 K_T + 1) \bar{C} + k_5)} - \epsilon,$$

$$K = \frac{K_T \bar{C}}{\frac{k_5}{k_4} + \bar{C}} + \epsilon, \quad K = \frac{K_T \bar{C}}{\frac{k_5}{k_4} + \bar{C}} - \epsilon.$$

To see this, we explicitly compute  $\bar{X} = (\bar{P}, \bar{K}, \bar{R}, \bar{C})$  by solving the following algebraic equations:

$$0 = \frac{k_1 \bar{C}}{(1 + k_2 \bar{K})} - k_3 \bar{P}, \quad (\text{C3})$$

$$0 = k_4 \bar{C} (K_T - \bar{K}) - k_5 \bar{K}, \quad (\text{C4})$$

$$0 = \frac{k_6 \bar{P} \bar{C}^2 (R_T - \bar{R})}{1 + k_7 \bar{P} (1 + k_8 \bar{C})} - k_9 \bar{R}, \quad (\text{C5})$$

$$0 = k_{10} \left( 1 + \frac{k_{11} \bar{P} \bar{C} (R_T - \bar{R})}{1 + k_7 \bar{P} (1 + k_8 \bar{C})} \right) (k_c - \bar{C}) - \frac{k_{12} \bar{C}^2}{\bar{C}^2 + k_{p2}^2}. \quad (\text{C6})$$

Beginning with Eq. (C4), by solving for  $\bar{K}$ ,

$$\bar{K} = \frac{K_T \bar{C}}{\frac{k_5}{k_4} + \bar{C}}. \quad (\text{C7})$$

This implies that the steady state of PKC follows sigmoidal or hyperbolic dose-response curve in  $\bar{C}$  in which the binding of a ligand to a single binding site is completely defined by the concentration of the binding site ( $B_{\text{max}} = K_T$ ) and the concentration of unbound ligand at which the binding site is 50% occupied [the equilibrium dissociation constant ( $K_d = k_5/k_4$ )]. Equation (C7) further indicates that

$(dK/dt) < 0$  on  $K = K_T \bar{C} / (k_5/k_4 + \bar{C}) + \epsilon$  and  $(dK/dt) > 0$  on  $K = K_T \bar{C} / (k_5/k_4 + \bar{C}) - \epsilon$ . Substituting Eq. (C7) into Eq. (C3), we also get

$$\bar{P} = \frac{k_1 \bar{C}}{k_3(1 + k_2 \bar{K})} = \frac{k_1 \bar{C}(k_4 \bar{C} + k_5)}{k_3(k_4(k_2 K_T + 1) \bar{C} + k_5)}, \quad (C8)$$

which implies that  $(dP/dt) < 0$  on  $P = k_1 \bar{C}(k_4 \bar{C} + k_5) / [k_3(k_4(k_2 K_T + 1) \bar{C} + k_5)] + \epsilon$  and  $(dP/dt) > 0$  on  $P$

eigenvalues are negative), ruling out the existence of any periodic orbit.

We further represent nullclines of  $C$  and  $R$  explicitly. By using Eq. (C8), from Eq. (C5),

$$f(\bar{C}, \bar{R}) \equiv \frac{k_6 P C^2 (R_T - R)}{1 + k_7 P (1 + k_8 C)} - k_9 R = 0,$$

$$\bar{R} = \frac{k_6 R_T \bar{P} \bar{C}}{k_9(1 + k_7 \bar{P}(1 + k_8 \bar{C})) + k_6 \bar{P} \bar{C}} = \frac{k_6 k_1 R_T \bar{C}^2 (k_4 \bar{C} + k_5)}{k_9(k_3(k_4(k_2 K_0 + 1) \bar{C} + k_5) + k_7 k_1 \bar{C}(k_4 \bar{C} + k_5)(1 + k_8 \bar{C})) + k_6 k_1 \bar{C}^2 (k_4 \bar{C} + k_5)}, \quad (C9)$$

which is a sigmoidal curve in  $C$ . Note that  $\bar{R}$  can be regarded as a function of  $k_1/k_2$  if we divide both denominator and numerator by  $k_1$ . Finally to get  $\bar{C}$ , if we rewrite Eq. (C6), as

$$g(\bar{C}, \bar{R}) \equiv k_{10} \left( 1 + \frac{k_9 k_{11} \bar{R}}{k_6} \right) (k_c - \bar{C}) - \frac{k_{12} \bar{C}^2}{\bar{C}^2 + k_{p2}^2} = 0. \quad (C10)$$

Equations (C9) and (C10) provide explicit expressions for  $\bar{C}$  versus  $\bar{R}$  so that we can plot the nullclines,  $dC/dt = 0$  and  $dR/dt = 0$ . For the  $C$  nullcline, if we solve Eq. (C10) for  $\bar{R}$ , then

$$\bar{R} = \frac{k_6}{k_9 k_{11}} \left( \frac{k_{12} C^2}{k_{10}(k_c - C)(C^2 + k_{p2}^2)} - 1 \right), \quad (C11)$$

$$g(\bar{C}, \bar{R}) \equiv \bar{R} - \frac{k_6}{k_9 k_{11}} \left( \frac{k_{12} C^2}{k_{10}(k_c - C)(C^2 + k_{p2}^2)} - 1 \right).$$

So far, it was shown that  $R-C$  system in Eq. (1) can have complex conjugate eigenvalues. Also, the nullclines of

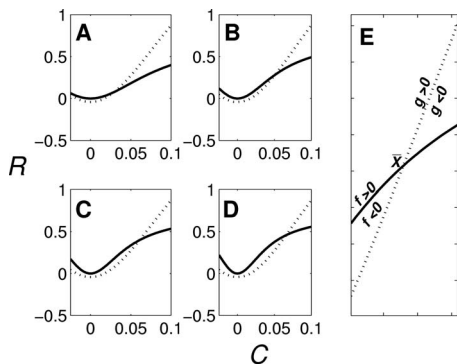


FIG. 10. Nullclines of  $C$  and  $R$  as  $k_1$  varies  $C$  nullcline [ $g(C, R) = 0$ : dotted line] and  $R$  nullcline [ $f(C, R) = 0$ : solid line]. [(a)–(d)]  $C-R$  nullclines for  $k_1 = 0.5, 1, 1.5,$  and  $2$ . (e)  $C-R$  nullclines near the steady state point ( $\bar{X}$ ).

$= k_1 \bar{C}(k_4 \bar{C} + k_5) / [k_3(k_4(k_2 K_T + 1) \bar{C} + k_5)] - \epsilon$ . Note that Eqs. (C7) and (C8) indicate that  $\bar{K} \approx \bar{C} \ll 1$  (even  $\bar{K} \approx 0$  for some  $k_5/k_4$ ) and  $\bar{P} \sim (k_1/k_3) \bar{C} + O(\bar{C}^2)$  for  $\bar{C} \ll 1$ , or  $\bar{P}$  as a function of  $k_1/k_3$  (i.e.,  $\bar{P} \approx \tilde{P}$  for some  $k_1/k_3$ ). Because  $\epsilon$  is an arbitrarily small positive number, we may assume that the invariant domain is a proper subset of the open set in which Eq. (C1) is oscillatory. This result further indicates that the steady state  $(\bar{P}, \bar{K})$  is stable (the real parts of associated

Eq. (1) can be reduced into manifolds in  $\bar{R}-\bar{C}$  space. By studying the local behavior of the  $R-C$  nullclines  $f(C, R) = 0$  and  $g(C, R) = 0$  at a steady state  $\bar{X}$ , we provide a condition for  $Ca_i^{2+}$  wave propagations in terms of  $k_1(A)$ .

Since the right-hand side of Eq. (C11) is independent of  $k_1$  as we can see from Figs. 10(a)–10(d),  $C$  nullcline ( $g(C, R) = 0$ ) does not change as  $k_1$  varies. Only  $R$  nullcline [ $f(C, R) = 0$ ] changes, i.e.,  $\bar{R}$  nullcline moves upward changing its curvature (and eigenvalues) as  $k_1$  (PLC activity) increases. Also, for  $\bar{X} = (\bar{C}, \bar{R})$ , both  $\bar{R}$  and  $\bar{C}$  increase as  $k_1$  increases.

Consider now Fig. 10(e). If the complex conjugate eigenvalues  $\lambda_1$  and  $\lambda_2$  are associated with  $\bar{X}$ ,  $\lambda_i, i = 1, 2$  satisfy

$$0 = |A - \lambda_i I|, A = \begin{bmatrix} \frac{\partial f}{\partial C} & \frac{\partial f}{\partial R} \\ \frac{\partial g}{\partial C} & \frac{\partial g}{\partial R} \end{bmatrix}.$$

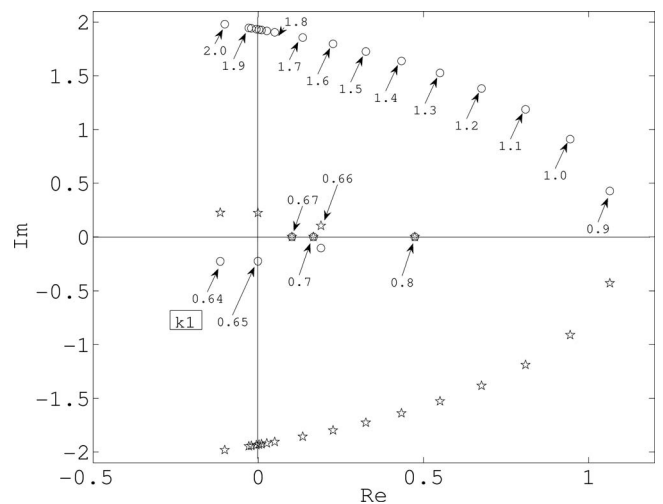


FIG. 11. Conjugate complex eigenvalues.

At the steady state  $\bar{X}$ ,  $\partial f/\partial C < 0$ ,  $\partial f/\partial R > 0$ , and  $\partial g/\partial C < 0$ ,  $\partial g/\partial R > 0$ , which indicates that the sign of  $\text{tr} A = \lambda_1 + \lambda_2 = \partial f/\partial C + \partial g/\partial R$  cannot be determined. Also, from  $dR/dC|_{g(C)=0} > dR/dC|_{f(C)=0}$ ,

$$\begin{aligned} \left. \frac{dR}{dC} \right|_{g(C)=0} &= -\frac{\partial g/\partial C}{\partial g/\partial R} > \left. \frac{dR}{dC} \right|_{f(C)=0} \\ &= -\frac{\partial f/\partial C}{\partial f/\partial R} \Rightarrow \lambda_1 \lambda_2 = \frac{\partial f}{\partial C} \frac{\partial g}{\partial R} - \frac{\partial f}{\partial R} \frac{\partial g}{\partial C} > 0, \end{aligned}$$

as expected from any complex conjugate eigenvalues.

To investigate how the sign of the real parts of the complex eigenvalues varies with respect to  $k_1(A)$ , the characteristic equation for  $D\Phi(\bar{X})$  ( $|D\Phi(\bar{X}) - \lambda I|$ ) was solved numerically. The numerical solution shows that there are two negative eigenvalues and a pair of conjugate complex eigenvalues. Figure 11 shows the location of conjugate eigenvalues in the complex plane. The stable steady state loses stability via a Hopf bifurcation as a pair of conjugate eigenvalues crosses the imaginary axis at  $k_1 = 0.65$ . At about 0.7 the pair merges to become real and remains so for  $k_1 = 0.7 - 0.9$ . Beyond  $k_1 \sim 0.9$ , these eigenvalues become complex and the steady state regains stability near  $k_1 = 1.85$ . This corresponds to the transient with plateau-type  $\text{Ca}_i^{2+}$  response.<sup>67</sup>

This result suggests that for  $\text{Ca}_i^{2+}$  waves to be propagated to the neighboring cells,  $k_1, k_{in}(B_{\max}A/K_d + A) > 0.6$  is required in each cells. However, under nonregenerative ATP release assumption, extracellular ATP is attenuated due to diffusion and enzymes as it propagates, and eventually  $k_{in}(B_{\max}A/K_d + A)$  becomes less than 0.6 ( $A < 2.5 \mu\text{M}$ ; recall that the effective ATP dosage was  $3 \mu\text{M}$ ), at which the real part of complex conjugate eigenvalues becomes negative.

<sup>1</sup>Agulhon, C., Petravic, J., McMullen, A. B., Sweger, E. J., Minton, S. K., Taves, S. R., Casper, K. B., Fiocco, T. A., and McCarthy, K. D., "What is the role of astrocyte calcium in neurophysiology?," *Neuron* **59**, 932–946 (2008).

<sup>2</sup>Anselmi, F., Hernandez, V. H., Crispino, G., Seydel, A., Ortolano, S., Roper, S. D., Kessaris, N., Richardson, W., Rickheit, G., Filippov, M. A., Monyer, H., and Mammiano, F., ATP release through connexin hemichannels and gap junction transfer of second messengers propagate  $\text{Ca}^{2+}$  signals across the inner ear," *Proc. Natl. Acad. Sci. U.S.A.* **105**, 18770–18775 (2008).

<sup>3</sup>Apolloni, S., Montilli, C., Finocchi, P., and Amadio, S., "Membrane compartments and purinergic signalling: P2x receptors in neurodegenerative and neuroinflammatory events," *FEBS J.* **276**, 354–364 (2009).

<sup>4</sup>Arcuino, G., Lin, J. H.-C., Takano, T., Liu, C., Jiang, L., Gao, Q., Kang, J., and Nedergaard, M., "Intercellular calcium signaling mediated by point-source burst release of ATP," *Proc. Natl. Acad. Sci. U.S.A.* **99**, 9840–9845 (2002).

<sup>5</sup>Aronson, D. G., Mantzaris, N. V., and Othmer, H. G., "Wave propagation and blocking in inhomogeneous media," *Discrete Contin. Dyn. Syst.* **13**, 843–876 (2005).

<sup>6</sup>Ashida, N., Ueyama, T., Rikitake, K., Shirai, Y., Eto, M., Kondoh, T., Kohmura, E., and Saito, N., " $\text{Ca}^{2+}$  oscillation induced by P2Y2 receptor activation and its regulation by a neuron-specific subtype of PKC (gammaPKC)," *Neurosci. Lett.* **446**, 123–128 (2008).

<sup>7</sup>Atri, A., Amundson, J., Clapham, D., and Sneyd, J., "A single-pool model for intracellular calcium oscillations and waves in the xenopus laevis oocyte," *Biophys. J.* **65**, 1727–1739 (1993).

<sup>8</sup>Babwah, A. V., Dale, L. B., and Ferguson, S. S. G., "Protein kinase C isoform-specific differences in the spatial-temporal regulation and decoding of metabotropic glutamate receptor1a-stimulated second messenger responses," *J. Biol. Chem.* **278**, 5419–5426 (2003).

<sup>9</sup>Barrow, S. L., Sherwood, M. W., Dolman, N. J., Gerasimenko, O. V., Voronina, S. G., and Tepikin, A. V., "Movement of calcium signals and calcium-binding proteins: Firewalls, traps and tunnels," *Biochem. Soc. Trans.* **34**, 381–384 (2006).

<sup>10</sup>Bartlett, P. J., Young, K. W., Nahorski, S. R., and Challiss, R. A. J., "Single cell analysis and temporal probing of agonist-mediated inositol 1,4,5-trisphosphate,  $\text{Ca}^{2+}$ , diacylglycerol, and protein kinase C signaling using fluorescent biosensors," *J. Biol. Chem.* **280**, 21837–21846 (2005).

<sup>11</sup>Bennett, M. R., Buljan, V., Farnell, L., and Gibson, W. G., "Purinergic junctional transmission and propagation of calcium waves in spinal cord astrocyte networks," *Biophys. J.* **91**, 3560–3571 (2006).

<sup>12</sup>Bennett, M. R., Farnell, L., and Gibson, W. G., "A quantitative model of cortical spreading depression due to purinergic and gap-junction transmission in astrocyte networks," *Biophys. J.* **95**, 5648–5660 (2008).

<sup>13</sup>Berridge, M. J., Bootman, M. D., and Lipp, P., "Calcium—A life and death signal," *Nature (London)* **395**, 645–648 (1998).

<sup>14</sup>Bezprozvanny, I., Watras, J., and Ehrlich, B. E., "Bell-shaped calcium-response curves of ins(1,4,5)p3- and calcium-gated channels from endoplasmic reticulum of cerebellum," *Nature (London)* **351**, 751–754 (1991).

<sup>15</sup>Blomstrand, F., Aberg, N. D., Eriksson, P. S., Hansson, E., and Rönnbäck, L., "Extent of intercellular calcium wave propagation is related to gap junction permeability and level of connexin-43 expression in astrocytes in primary cultures from four brain regions," *Neuroscience* **92**, 255–265 (1999).

<sup>16</sup>Bobalova, J. and Mutafova-Yambolieva, V. N., "Co-release of endogenous ATP and noradrenaline from guinea-pig mesenteric veins exceeds co-release from mesenteric arteries," *Clin. Exp. Pharmacol. Physiol.* **28**, 397–401 (2001).

<sup>17</sup>Bowser, D. N. and Khakh, B. S., "Two forms of single-vesicle astrocyte exocytosis imaged with total internal reflection fluorescence microscopy," *Proc. Natl. Acad. Sci. U.S.A.* **104**, 4212–4217 (2007).

<sup>18</sup>Bowser, D. N. and Khakh, B. S., "Vesicular ATP is the predominant cause of intercellular calcium waves in astrocytes," *J. Gen. Physiol.* **129**, 485–491 (2007).

<sup>19</sup>Braet, K., Aspeslagh, S., Vandamme, W., Willecke, K., Martin, P. E. M., Evans, W. H., and Leybaert, L., "Pharmacological sensitivity of ATP release triggered by photoliberation of inositol-1,4,5-trisphosphate and zero extracellular calcium in brain endothelial cells," *J. Cell Physiol.* **197**, 205–213 (2003).

<sup>20</sup>Braet, K., Vandamme, W., Martin, P. E. M., Evans, W. H., and Leybaert, L., "Photoliberating inositol-1,4,5-trisphosphate triggers ATP release that is blocked by the connexin mimetic peptide gap 26," *Cell Calcium* **33**, 37–48 (2003).

<sup>21</sup>Bushong, E. A., Martone, M. E., Jones, Y. Z., and Ellisman, M. H., "Protoplasmic astrocytes in CA1 stratum radiatum occupy separate anatomical domains," *J. Neurosci.* **22**, 183–192 (2002).

<sup>22</sup>Coco, S., Calegari, F., Pravettoni, E., Pozzi, D., Taverna, E., Rosa, P., Matteoli, M., and Verderio, C., "Storage and release of ATP from astrocytes in culture," *J. Biol. Chem.* **278**, 1354–1362 (2003).

<sup>23</sup>Codazzi, F., Teruel, M. N., and Meyer, T., "Control of astrocyte  $\text{Ca}^{2+}$  oscillations and waves by oscillating translocation and activation of protein kinase C," *Curr. Biol.* **11**, 1089–1097 (2001).

<sup>24</sup>Cornell-Bell, A. H., Finkbeiner, S. M., Cooper, M. S., and Smith, S. J., "Glutamate induces calcium waves in cultured astrocytes: Long-range glial signaling," *Science* **247**, 470–473 (1990).

<sup>25</sup>Cotrina, M. L., Lin, J. H., Alves-Rodrigues, A., Liu, S., Li, J., Azmi-Ghadimi, H., Kang, J., Naus, C. C., and Nedergaard, M., "Connexins regulate calcium signaling by controlling ATP release," *Proc. Natl. Acad. Sci. U.S.A.* **95**, 15735–15740 (1998).

<sup>26</sup>Cotrina, M. L., Lin, J. H.-C., López-García, J. C., Naus, C. C. G., and Nedergaard, M., "ATP-mediated glia signaling," *J. Neurosci.* **20**, 2835–2844 (2000).

<sup>27</sup>Cotrina, M. L., Lin, J. H.-C., and Nedergaard, M., "Cytoskeletal assembly and ATP release regulate astrocytic calcium signaling," *J. Neurosci.* **18**, 8794–8804 (1998).

<sup>28</sup>Cunningham, M. L., Filtz, T. M., and Harden, T. K., "Protein kinase C-promoted inhibition of galph(11)-stimulated phospholipase C-beta activity," *Mol. Pharmacol.* **56**, 265–271 (1999).

<sup>29</sup>Dale, L. B., Babwah, A. V., Bhattacharya, M., Kelvin, D. J., and Ferguson, S. S., "Spatial-temporal patterning of metabotropic glutamate receptor-mediated inositol 1,4,5-trisphosphate, calcium, and protein kinase C oscillations: Protein kinase C-dependent receptor phosphorylation is not required," *J. Biol. Chem.* **276**, 35900–35908 (2001).

<sup>30</sup>Dale, L. B., Babwah, A. V., and Ferguson, S. S. G., "Mechanisms of metabotropic glutamate receptor desensitization: Role in the patterning of

- ector enzyme activation," *Neurochem. Int.* **41**, 319–326 (2002).
- <sup>31</sup>Dale, L. B., Bhattacharya, M., Anborgh, P. H., Murdoch, B., Bhatia, M., Nakanishi, S., and Ferguson, S. S., "G protein-coupled receptor kinase-mediated desensitization of metabotropic glutamate receptor 1a protects against cell death," *J. Biol. Chem.* **275**, 38213–38220 (2000).
- <sup>32</sup>Davalos, D., Grutzendler, J., Yang, G., Kim, J. V., Zuo, Y., Jung, S., Littman, D. R., Dustin, M. L., and Gan, W. B., "ATP mediates rapid microglial response to local brain injury *in vivo*," *Nat. Neurosci.* **8**, 752–758 (2005).
- <sup>33</sup>Davis, T. and Duff, I., "An unsymmetric-pattern multifrontal method for sparse LU factorization," *SIAM J. Matrix Anal. Appl.* **18**, 140–158 (1997).
- <sup>34</sup>Delicado, E., Jimenez, A., Carrasquero, L., Castro, E., and Miras-Portugal, M., "Cross-talk among epidermal growth factor, ap (5) a, and nucleotide receptors causing enhanced ATP Ca<sup>2+</sup> signaling involves extracellular kinase activation in cerebellar astrocytes," *J. Neurosci. Res.* **81**, 789–796 (2005).
- <sup>35</sup>Ding, S., Fellin, T., Zhu, Y., Lee, S. Y., Auberson, Y. P., Meaney, D. F., Coulter, D. A., Carmignoto, G., and Haydon, P. G., "Enhanced astrocytic Ca<sup>2+</sup> signals contribute to neuronal excitotoxicity after status epilepticus," *J. Neurosci.* **27**, 10674–10684 (2007).
- <sup>36</sup>Dokukina, I., Gracheva, M., Grachev, E., and Gunton, J., "Role of network connectivity in intercellular calcium signaling," *Physica D* **237**, 745–754 (2008).
- <sup>37</sup>Dupont, G., Combettes, L., and Leybaert, L., "Calcium dynamics: Spatio-temporal organization from the subcellular to the organ level," *Int. Rev. Cytol.* **261**, 193–245 (2007).
- <sup>38</sup>Dupont, G. and Goldbeter, A., "Oscillations and waves of cytosolic calcium: Insights from theoretical models," *BioEssays* **14**, 485–493 (1992).
- <sup>39</sup>Dupont, G. and Goldbeter, A., "Properties of intracellular Ca<sup>2+</sup> waves generated by a model based on Ca<sup>2+</sup>-induced Ca<sup>2+</sup> release," *Biophys. J.* **67**, 2191–2204 (1994).
- <sup>40</sup>Espallergues, J., Solovieva, O., Técher, V., Bauer, K., Alonso, G., Vincent, A., and Hussy, N., "Synergistic activation of astrocytes by ATP and norepinephrine in the rat supraoptic nucleus," *Neuroscience* **148**, 712–723 (2007).
- <sup>41</sup>Falcke, M., Li, Y., Lechleiter, J. D., and Camacho, P., "Modeling the dependence of the period of intracellular Ca<sup>2+</sup> waves on serca expression," *Biophys. J.* **85**, 1474–1481 (2003).
- <sup>42</sup>Fall, C. P., Wagner, J. M., Loew, L. M., and Nuccitelli, R., "Cortically restricted production 1 of IP<sub>3</sub> leads to propagation of the fertilization Ca<sup>2+</sup> wave along the cell surface in a model of the xenopus egg," *J. Theor. Biol.* **231**, 487–496 (2004).
- <sup>43</sup>Fiacco, T. A., Agulhon, C., Taves, S. R., Petravic, J., Casper, K. B., Dong, X., Chen, J., and McCarthy, K. D., "Selective stimulation of astrocyte calcium *in situ* does not affect neuronal excitatory synaptic activity," *Neuron* **54**, 611–626 (2007).
- <sup>44</sup>Fiacco, T. A. and McCarthy, K. D., "Intracellular astrocyte calcium waves *in situ* increase the frequency of spontaneous ampa receptor currents in CA1 pyramidal neurons," *J. Neurosci.* **24**, 722–732 (2004).
- <sup>45</sup>Fiacco, T. A. and McCarthy, K. D., "Astrocyte calcium elevations: Properties, propagation, and effects on brain signaling," *Glia* **54**, 676–690 (2006).
- <sup>46</sup>Filtz, T. M., Cunningham, M. L., Stanig, K. J., Paterson, A., and Harden, T. K., "Phosphorylation by protein kinase C decreases catalytic activity of avian phospholipase C-beta," *Biochem. J.* **338**, 257–264 (1999).
- <sup>47</sup>Fowler, A. C., *Mathematical Models in the Applied Sciences* (Cambridge University Press, Cambridge, UK, 1997).
- <sup>48</sup>Franke, H., Krügel, U., Grosche, J., Heine, C., Härtig, W., Allgaier, C., and Illes, P., "P2Y receptor expression on astrocytes in the nucleus accumbens of rats," *Neuroscience* **127**, 431–441 (2004).
- <sup>49</sup>Giaume, C. and Venance, L., "Intercellular calcium signaling and gap junctional communication in astrocytes," *Glia* **24**, 50–64 (1998).
- <sup>50</sup>Gordon, J. L., "Extracellular ATP: effects, sources and fate," *Biochem. J.* **233**, 309–319 (1986).
- <sup>51</sup>Gribble, F. M., Loussouarn, G., Tucker, S. J., Zhao, C., Nichols, C. G., and Ashcroft, F. M., "A novel method for measurement of submembrane ATP concentration," *J. Biol. Chem.* **275**, 30046–30049 (2000).
- <sup>52</sup>Griffith, D. A. and Jarvis, S. M., "Nucleoside and nucleobase transport systems of mammalian cells," *Biochim. Biophys. Acta* **1286**, 153–181 (1996).
- <sup>53</sup>Guan, X., Cravatt, B. F., Ehring, G. R., Hall, J. E., Boger, D. L., Lerner, R. A., and Gilula, N. B., "The sleep-inducing lipid oleamide deconvolutes gap junction communication and calcium wave transmission in glial cells," *J. Cell Biol.* **139**, 1785–1792 (1997).
- <sup>54</sup>Guthrie, P. B., Knappenberger, J., Segal, M., Bennett, M. V. L., Charles, A. C., and Kater, S. B., "ATP released from astrocytes mediates glial calcium waves," *J. Neurosci.* **19**, 520–528 (1999).
- <sup>55</sup>Hall, J., *Guyton Physiology Review* (Saunders, 2005).
- <sup>56</sup>Hamilton, N., Vayro, S., Kirchoff, F., Verkhratsky, A., Robbins, J., Gorecki, D., and Butt, A., "Mechanisms of ATP-and glutamate-mediated calcium signaling in white matter astrocytes," *Glia* **56**, 734–749 (2008).
- <sup>57</sup>Harris-White, M. E., Zanotti, S. A., Frautschy, S. A., and Charles, A. C., "Spiral intercellular calcium waves in hippocampal slice cultures," *J. Neurophysiol.* **79**, 1045–1052 (1998).
- <sup>58</sup>Hassinger, T. D., Guthrie, P. B., Atkinson, P. B., Bennett, M. V., and Kater, S. B., "An extracellular signaling component in propagation of astrocytic calcium waves," *Proc. Natl. Acad. Sci. U.S.A.* **93**, 13268–13273 (1996).
- <sup>59</sup>Hubley, M. J., Locke, B. R., and Moerland, T. S., "The effects of temperature, pH, and magnesium on the diffusion coefficient of ATP in solutions of physiological ionic strength," *Biochim. Biophys. Acta* **1291**, 115–121 (1996).
- <sup>60</sup>Höfer, T., Venance, L., and Giaume, C., "Control and plasticity of intercellular calcium waves in astrocytes: A modeling approach," *J. Neurosci.* **22**, 4850–4859 (2002).
- <sup>61</sup>Jafri, M. S. and Keizer, J., "On the roles of Ca<sup>2+</sup> diffusion, Ca<sup>2+</sup> buffers, and the endoplasmic reticulum in IP<sub>3</sub>-induced Ca<sup>2+</sup> waves," *Biophys. J.* **69**, 2139–2153 (1995).
- <sup>62</sup>Jafri, M. S. and Keizer, J., "Agonist-induced calcium waves in oscillatory cells: A biological example of Burgers' equation," *Bull. Math. Biol.* **59**, 1125–1144 (1997).
- <sup>63</sup>John, G. R., Scemes, E., Suadicani, S. O., Liu, J. S., Charles, P. C., Lee, S. C., Spray, D. C., and Brosnan, C. F., "IL-1beta differentially regulates calcium wave propagation between primary human fetal astrocytes via pathways involving P2 receptors and gap junction channels," *Proc. Natl. Acad. Sci. U.S.A.* **96**, 11613–11618 (1999).
- <sup>64</sup>Joseph, S. M., Buchakjian, M. R., and Dubyak, G. R., "Colocalization of ATP release sites and ecto-ATPase activity at the extracellular surface of human astrocytes," *J. Biol. Chem.* **278**, 23331–23342 (2003).
- <sup>65</sup>Kang, J., Kang, N., Lovatt, D., Torres, A., Zhao, Z., Lin, J., and Nedergaard, M., "Connexin 43 hemichannels are permeable to ATP," *J. Neurosci.* **28**, 4702–4711 (2008).
- <sup>66</sup>Kang, M., "Temporal and spatial aspects of calcium dynamics in astrocytes," Ph.D. thesis, University of Minnesota, 2004.
- <sup>67</sup>Kang, M. and Othmer, H. G., "The variety of cytosolic calcium responses and possible roles of PLC and PKC," *Phys. Biol.* **4**, 325–343 (2007).
- <sup>68</sup>Katsuragi, T., Sato, C., Usune, S., Ueno, S., Segawa, M., and Migita, K., "Caffeine-inducible ATP release is mediated by Ca<sup>2+</sup>-signal transducing system from the endoplasmic reticulum to mitochondria," *Naunyn-Schmiedeberg's Arch. Pharmacol.* **378**, 93–101 (2008).
- <sup>69</sup>Kawano, S., Otsu, K., Kuruma, A., Shoji, S., Yanagida, E., Muto, Y., Yoshikawa, F., Hirayama, Y., Mikoshiba, K., and Furuichi, T., "ATP autocrine/paracrine signaling induces calcium oscillations and NFAT activation in human mesenchymal stem cells," *Cell Calcium* **39**, 313–324 (2006).
- <sup>70</sup>Keener, J. and Sneyd, J., *Mathematical Physiology* (Springer, Berlin, 2001).
- <sup>71</sup>Kimelberg, H. K., "Increased release of excitatory amino acids by the actions of ATP and peroxy-nitrite on volume-regulated anion channels (VRACs) in astrocytes," *Neurochem. Int.* **45**, 511–519 (2004).
- <sup>72</sup>Konietzko, U. and Müller, C. M., "Astrocytic dye coupling in rat hippocampus: Topography, developmental onset, and modulation by protein kinase C," *Hippocampus* **4**, 297–306 (1994).
- <sup>73</sup>Lazarowski, E. R., Watt, W. C., Stutts, M. J., Boucher, R. C., and Harden, T. K., "Pharmacological selectivity of the cloned human P2U-purinoceptor: potent activation by diadenosine tetraphosphate," *Br. J. Pharmacol.* **116**, 1619–1627 (1995).
- <sup>74</sup>MacDonald, C. L., Yu, D., Buibas, M., and Silva, G. A., "Diffusion modeling of ATP signaling suggests a partially regenerative mechanism underlying astrocyte intercellular calcium waves," *Front. Neuroeng.* **1**, 1–13 (2008).
- <sup>75</sup>Mazel, T., Richter, F., Vargová, L., and Syková, E., "Changes in extracellular space volume and geometry induced by cortical spreading depression in immature and adult rats," *Physiol. Res.* **51**, S85–S93 (2002).
- <sup>76</sup>Merten, M. D., Saleh, A., Kammouni, W., Marchand, S., and Figarella, C., "Characterization of two distinct P2Y receptors in human tracheal gland cells," *Eur. J. Biochem.* **251**, 19–24 (1998).
- <sup>77</sup>Mongin, A. A. and Kimelberg, H. K., "ATP potently modulates anion channel-mediated excitatory amino acid release from cultured astrocytes," *Am. J. Physiol.: Cell Physiol.* **283**, C569–C578 (2002).

- <sup>78</sup>Nadkarni S., Jung P., and Levine H., "Astrocytes optimize the synaptic transmission of information," *PLOS Comput. Biol.* **4**, e1000088 (2008).
- <sup>79</sup>Nagy, J. I. and Rash, J. E., "Connexins and gap junctions of astrocytes and oligodendrocytes in the CNS," *Brain Res. Rev.* **32**, 29–44 (2000).
- <sup>80</sup>Nash, M. S., Schell, M. J., Atkinson, P. J., Johnston, N. R., Nahorski, S. R., and Challiss, R. A. J., "Determinants of metabotropic glutamate receptor-5-mediated  $Ca^{2+}$  and inositol 1,4,5-trisphosphate oscillation frequency. Receptor density versus agonist concentration," *J. Biol. Chem.* **277**, 35947–35960 (2002).
- <sup>81</sup>Newman, E. A., Glial cells of the rat retina (<http://www.manticmoo.com/articles/jeff/programming/latex/bibtexstyles.php>).
- <sup>82</sup>Newman, E. A., "Propagation of intercellular calcium waves in retinal astrocytes and Müller cells," *J. Neurosci.* **21**, 2215–2223 (2001).
- <sup>83</sup>Ni, Y., Malarkey, E. B., and Parpura, V., "Vesicular release of glutamate mediates bidirectional signaling between astrocytes and neurons," *J. Neurochem.* **103**, 1273–1284 (2007).
- <sup>84</sup>Zur Nieden, R. Z. and Deitmer, J. W., "The role of metabotropic glutamate receptors for the generation of calcium oscillations in rat hippocampal astrocytes *in situ*," *Cereb. Cortex* **16**, 676–687 (2006).
- <sup>85</sup>Oberheim, N. A., Wang, X., Goldman, S., and Nedergaard, M., "Astrocytic complexity distinguishes the human brain," *Trends Neurosci.* **29**, 547–553 (2006).
- <sup>86</sup>Piet, R. and Jahr, C. E., "Glutamatergic and purinergic receptor-mediated calcium transients in Bergmann glial cells," *J. Neurosci.* **27**, 4027–4035 (2007).
- <sup>87</sup>Piet, R., Vargová, L., Syková, E., Poulain, D. A., and Oliet, S. H. R., "Physiological contribution of the astrocytic environment of neurons to intersynaptic crosstalk," *Proc. Natl. Acad. Sci. U.S.A.* **101**, 2151–2155 (2004).
- <sup>88</sup>De Pittà, M. D., Volman, V., Levine, H., Pioggia, G., Rossi, D. D., and Ben-Jacob, E., "Coexistence of amplitude and frequency modulations in intracellular calcium dynamics," *Phys. Rev. E* **77**, 030903(R) (2008).
- <sup>89</sup>Porter, J. T. and McCarthy, K. D., "Astrocytic neurotransmitter receptors *in situ* and *in vivo*," *Prog. Neurobiol.* **51**, 439–455 (1997).
- <sup>90</sup>Ralevic, V. and Burnstock, G., "Receptors for purines and pyrimidines," *Pharmacol. Rev.* **50**, 413–492 (1998).
- <sup>91</sup>Rostovtseva, T. K. and Bezrukov, S. M., "ATP transport through a single mitochondrial channel, VDAC, studied by current fluctuation analysis," *Biophys. J.* **74**, 2365–2373 (1998).
- <sup>92</sup>Sabirov, R. Z., Dutta, A. K., and Okada, Y., "Volume-dependent ATP-conductive large-conductance anion channel as a pathway for swelling-induced ATP release," *J. Gen. Physiol.* **118**, 251–266 (2001).
- <sup>93</sup>Sanderson, M. J., Charles, A. C., Boitano, S., and Dirksen, E. R., "Mechanisms and function of intercellular calcium signaling," *Mol. Cell Endocrinol.* **98**, 173–187 (1994).
- <sup>94</sup>Scemes, E., "Components of astrocytic intercellular calcium signaling," *Mol. Neurobiol.* **22**, 167–179 (2000).
- <sup>95</sup>Scemes, E. and Giaume, C., "Astrocyte calcium waves: What they are and what they do," *Glia* **54**, 716–725 (2006).
- <sup>96</sup>Sedaa, K. O., Bjur, R. A., Shinozuka, K., and Westfall, D. P., "Nerve and drug-induced release of adenine nucleosides and nucleotides from rabbit aorta," *J. Pharmacol. Exp. Ther.* **252**, 1060–1067 (1990).
- <sup>97</sup>Shelton, M. K. and McCarthy, K. D., "Hippocampal astrocytes exhibit  $Ca^{2+}$ -elevating muscarinic cholinergic and histaminergic receptors *in situ*," *J. Neurochem.* **74**, 555–563 (2000).
- <sup>98</sup>Shinozuka, K., Hashimoto, M., Masumura, S., Bjur, R. A., Westfall, D. P., and Hattori, K., "In vitro studies of release of adenine nucleotides and adenosine from rat vascular endothelium in response to alpha 1-adrenoceptor stimulation," *Br. J. Pharmacol.* **113**, 1203–1208 (1994).
- <sup>99</sup>Silchenko, A. N. and Tass, P. A., "Computational modeling of paroxysmal depolarization shifts in neurons induced by the glutamate release from astrocytes," *Biol. Cybern.* **98**, 61–74 (2008).
- <sup>100</sup>Sneyd, J., Girard, S., and Clapham, D., "Calcium wave propagation by calcium-induced calcium release: An unusual excitable system," *Bull. Math. Biol.* **55**, 315–344 (1993).
- <sup>101</sup>Stamatakis, M. and Mantzaris, N. V., "Modeling of ATP-mediated signal transduction and wave propagation in astrocytic cellular networks," *J. Theor. Biol.* **241**, 649–668 (2006).
- <sup>102</sup>Stamatakis, M. and Mantzaris, N. V., "Astrocyte signaling in the presence of spatial inhomogeneities," *Chaos* **17**, 033123-1–033123-12 (2007).
- <sup>103</sup>Stout, C. E., Costantin, J. L., Naus, C. C. G., and Charles, A. C., "Intercellular calcium signaling in astrocytes via ATP release through connexin hemichannels," *J. Biol. Chem.* **277**, 10482–10488 (2002).
- <sup>104</sup>Suadicani, S. O., Brosnan, C. F., and Scemes, E., "P2x7 receptors mediate ATP release and amplification of astrocytic intercellular  $Ca^{2+}$  signaling," *J. Neurosci.* **26**, 1378–1385 (2006).
- <sup>105</sup>Suadicani, S. O., Flores, C. E., Urban-Maldonado, M., Beelitz, M., and Scemes, E., "Gap junction channels coordinate the propagation of intercellular  $Ca^{2+}$  signals generated by P2y receptor activation," *Glia* **48**, 217–229 (2004).
- <sup>106</sup>Sykova, E., "The extracellular space in the CNS: Its regulation, volume and geometry in normal and pathological neuronal function," *Neuroscientist* **3**, 28–41 (1997).
- <sup>107</sup>Tang, Y. and Othmer, H. G., "Frequency encoding in excitable systems with applications to calcium oscillations," *Proc. Natl. Acad. Sci. U.S.A.* **92**, 7869–7873 (1995).
- <sup>108</sup>Taufik, E. and Probert, L., "Ischemic neuronal damage," *Curr. Pharm. Des.* **14**, 3565–3573 (2008).
- <sup>109</sup>Taylor, A. L., Kudlow, B. A., Marrs, K. L., Gruenert, D. C., Guggino, W. B., and Schwiebert, E. M., "Bioluminescence detection of ATP release mechanisms in epithelia," *Am. J. Physiol.* **275**, C1391–C1406 (1998).
- <sup>110</sup>Thul, R., Bellamy, T. C., Roderick, H. L., Bootman, M. D., and Coombes, S., "Calcium oscillations," *Adv. Exp. Med. Biol.* **641**, 1–27 (2008).
- <sup>111</sup>Tordjmann, T., Berthon, B., Claret, M., and Combettes, L., "Coordinated intercellular calcium waves induced by noradrenaline in rat hepatocytes: Dual control by gap junction permeability and agonist," *EMBO J.* **16**, 5398–5407 (1997).
- <sup>112</sup>Uchino, M., Sakai, N., Kashiwagi, K., Shirai, Y., Shinohara, Y., Hirose, K., Iino, M., Yamamura, T., and Saito, N., "Isoform-specific phosphorylation of metabotropic glutamate receptor 5 by protein kinase C (PKC) blocks  $Ca^{2+}$  oscillation and oscillatory translocation of  $Ca^{2+}$ -dependent PKC," *J. Biol. Chem.* **279**, 2254–2261 (2004).
- <sup>113</sup>Venance, L., Stella, N., Glowinski, J., and Giaume, C., "Mechanism involved in initiation and propagation of receptor-induced intercellular calcium signaling in cultured rat astrocytes," *J. Neurosci.* **17**, 1981–1992 (1997).
- <sup>114</sup>Verkhatsky, A. and Kettenmann, H., "Calcium signalling in glial cells," *Trends Neurosci.* **19**, 346–352 (1996).
- <sup>115</sup>Verkhatsky, A., Orkand, R. K., and Kettenmann, H., "Glial calcium: homeostasis and signaling function," *Physiol. Rev.* **78**, 99–141 (1998).
- <sup>116</sup>Volman, V., Ben-Jacob, E., and Levine, H., "The astrocyte as a gatekeeper of synaptic information transfer," *Neural Comput.* **19**, 303–326 (2007).
- <sup>117</sup>Volterra, A. and Meldolesi, J., "Astrocytes, from brain glue to communication elements: The revolution continues," *Nat. Rev. Neurosci.* **6**, 626–640 (2005).
- <sup>118</sup>De Vuyst, E. D., Decrock, E., Cabooter, L., Dubyak, G. R., Naus, C. C., Evans, W. H., and Leybaert, L., "Intracellular calcium changes trigger connexin hemichannel opening," *EMBO J.* **25**, 34–44 (2006).
- <sup>119</sup>Wagner, J., Li, Y. X., Pearson, J., and Keizer, J., "Simulation of the fertilization  $Ca^{2+}$  wave in xenopus laevis eggs," *Biophys. J.* **75**, 2088–2097 (1998).
- <sup>120</sup>Wang, Z., Haydon, P. G., and Yeung, E. S., "Direct observation of calcium-independent intercellular ATP signaling in astrocytes," *Anal. Chem.* **72**, 2001–2007 (2000).
- <sup>121</sup>Wilson, P. D., Hovater, J. S., Casey, C. C., Fortenberry, J. A., and Schwiebert, E. M., "ATP release mechanisms in primary cultures of epithelia derived from the cysts of polycystic kidneys," *J. Am. Soc. Nephrol.* **10**, 218–229 (1999).
- <sup>122</sup>Zhang, Z., Chen, G., Zhou, W., Song, A., Xu, T., Luo, Q., Wang, W., Gu, X., and Duan, S., "Regulated ATP release from astrocytes through lysosome exocytosis," *Nat. Cell Biol.* **9**, 945–953 (2007).
- <sup>123</sup>Zhao, Y., Migita, K., Sato, C., Usune, S., Iwamoto, T., and Katsuragi, T., "Endoplasmic reticulum is a key organella in bradykinin-triggered ATP release from cultured smooth muscle cells," *J. Pharmacol. Sci.* **105**, 57–65 (2007).